# FIREURISK - DEVELOPING A HOLISTIC, RISK-WISE STRATEGY FOR EUROPEAN WILDFIRE MANAGEMENT


| | |
|---|---|
| **Grant Agreement Number: 101003890**<br>**Call identifier:** H2020-LC-CLA-2018-2019-2020 | |
| **Topic:** | LC-CLA-15-2020<br>Forest Fires risk reduction: towards an integrated fire management approach in the E.U. |
| **Instrument:** | RIA |


# D3.3 – Improved fire regime simulations using hybrid functions in fire models and in fire-enabled DGVMs

This project has received funding from the European Union's Horizon 2020 research and innovation programme under grant agreement No 101003890.

| | |
|---|---|
| **Deliverable Identifier:** | D3.3 |
| **Deliverable Due Date:** | 30/11/2022 |
| **Deliverable Submission Date:** | 31/01/2023 |
| **Deliverable Version:** | 01 |
| **Lead partner:** | TUD |
| **Authors:** | Jessica Hetzer (SGN), Thomas Hickler (SGN), Eric Kosczor (TUD), Matthias Forkel (TUD), Kirsten Thonicke (PIK), Maik Billing (PIK), Simon Bowring (LSCE), Florent Mouillot (IRD), Evgenii Antonov (FMI), Mikhail Sofiev (FMI) |
| **Work Package:** | WP3 – Adaptation to future fire risk conditions |
| **Task:** | Task 3.1 - Generate future scenario data for the three spatial scales |
| **Dissemination Level:** | ☐ PU: Public<br>☒ CO: Confidential, only for members of the Consortium (including the Commission Services) |

# Revision History

| Version | Date | Edited by | Description |
|---|---|---|---|
| v.0.1 | 01/11/2022 | SGN, PIK, TUD | Document Content outline / structure |
| v.0.2 | 01/12/2022 | SGN, PIK, TUD, LSCE, IDR, FMI | Draft version |
| v.0.3 | 19/12/22 | SGN | Complete version formatted according to template |
| v.0.4 | 19/12/22 | SGN | Complete version with Annexes |
| v.0.5 | | | Complete draft review by WP3 Leader |
| v.0.6 | | | Internal review of the Complete version |
| v.0.9 | 17/01/23 | SHD | Internal approval review by the QRB |
| v.1.0 | 25/01/23 | SGN | Final version submitted |

# Quality Control

| Type | Date | Reviewed by | Approved/Comment |
|---|---|---|---|
| Peer | 17/01/2023 | S. Doerr | Very minor edits suggested |
| Internal Review | 17/01/2023 | Vasileios Kazoukas | Security Officer: approved |
| | | | |

## Executive Summary

The deliverable reports improvements of fire-enabled vegetation models, with a particular focus to improve so far poorly represented on processes. Most processes in fire enabled vegetation models are parameterized based on biophysical process understanding, but this approach has limits because socio-economic factors are crucial for understanding fire ignitions and spread. Therefore, we aimed at introducing hybrid modelling, whereby functions for human ignitions were parameterized with machine learning techniques (chapter 2). We also improved model representations for other important processes, such as predictions of main tree species (fuel characteristics), crown fire spread and fragmentation effects, which are crucial for simulating extreme fires, and finally, a system for projecting future fire danger.

The new human ignition functions were implemented and tested in two fire-enabled dynamic global vegetation models (DGVMs), LPJmL5.1-SPITFIRE and LPJ-GUESS-SPITFIRE (chapter 3). Comparisons at the scale of Europe were carried out with LPJmL5.1-SPITFIRE and improved the model results for burned area. First results of LPJ-GUESS-SPITFIRE are in line with these findings. In the vegetation model ORCHIDEE-SPITFIRE, new functions for simulating crown fires and fragmentation, lead to improved results, in particular concerning crown fires (chapter 4). New drivers were evaluated in the Integrated System for Wildland Fires (IS4FIRES, chapter 5). And finally, to gain deeper insights in fuel characteristics regarding the species composition, the representation of species reproduction success and subsequent species distribution was analyzed by the process-based Phenofit-SIERRA (chapter 6). All these model developments will contribute to improved future predictions of task 3.1.

### *Disclaimer*



### *Copyright message*

# Table of Contents



 

| Abbreviations | |
|---|---|
| AUC | Area under the curve |
| BOEU | Boreal Eurasia |
| BONA | Boreal N. America |
| CESM | Community Earth System Model |
| CMA-ES | Covariance Matrix Adaptation Evolution Strategy |
| DGVM | Dynamic global vegetation models |
| ERA | European Reanalysis |
| FDI | Fire danger indices |
| FFM | Fire Forecasting Model |
| GCM | Global Circulation Model |
| GENOUD | Genetic Optimization Using Derivatives |
| GFED | Global Fire Emissions Database |
| IS4FIRES | Integrated System for vegetation fires |
| LAEA | Lambert Azimuthal Equal Area |
| LPJ-GUESS | Lund–Potsdam–Jena General Ecosystem Simulator |
| LPJmL | Lund-Potsdam-Jena managed Land |
| MODIS | Moderate-resolution Imaging Spectroradiometer |
| ORCHIDEE | Organising Carbon and Hydrology In Dynamic Ecosystems |
| PDP | Partial dependence plot |
| PFT | Plant functional type |
| Phenofit | Remote sensing vegetation phenology extraction package |
| RF | Random forest |
| SOFIA | Satellite Observations to predict FIre Activity |
| SPITFIRE | Spread and InTensity of FIRE fire model |
| SSE | Sum of squared error |

# 1 Introduction

## 1.1 Purpose

The main objective of this deliverable is to "Improve fire regime simulations using hybrid functions in fire models and in fire-enabled DGVMs (D.3.3)". The studies that have been carried out used commonly used fire-enabled dynamic vegetation models (DGVMs) together with high-resolution climate data, that was provided by earlier deliverables of this task. All work that was contributed to this deliverable had a substantial part in improving model approaches or fuel representation and to prepare Task 3.1 for improved future simulations.

## 1.2 State of the art

Fire-enabled DGVMs are becoming increasingly important for understanding interactions between vegetation and fire and to predict fire behavior and effects. Crucial processes, in particular related to human influences, such as **human fire ignition** or landscape fragmentation, can hardly be parameterized based on biophysical processes alone. Here more empirical machine learning approaches are thought to have a lot of potential.

Recent studies have shown that human caused ignitions depend highly on socio-economical or landscape related variables such as GDP or distance to wildland-urban interfaces. This is particularly important in an area as highly characterized by cultural landscapes such as Europe. In contrast to these findings, potential human ignitions in the widely used SPITFIRE model only depend on an empirical relation to local population density (Thonicke et al., 2010). Therefore, replacing the original SPITFIRE approach with the more complex SOFIA hybrid function approach has been one of our priorities. As natural **ignitions by lightning** also are very relevant in some regions of Europe, improving their prediction has also been addressed in our work.

Another priority has been to improve the representation of **extreme fires**, which are likely to increase in most areas of Europe. The area affected by extreme fires is thought to depend highly on **landscape fragmentation**, which is also purely captured in current fire-enabled DGVMs. Finally, the reliability of predictions with fire-enabled vegetation models also depends on the quality of the vegetation predictions, for example the simulated **distributions of major tree species**. Therefore, we also aimed at improving the process-based species distribution model PHENOFIT.

## 1.3 Structure of the report

During the reporting period, we identified the need for improvements regarding socio-economic influences on fire. Participants developed machine-learning approaches and gained new insights for modelling human ignitions (chapter 2). Derived empirical functions have been implemented and tested in the fire-enabled DGVMs, LPJmL5.1-SPITFIRE and LPJ-GUESS-SPITFIRE (chapter 3). The deliverable includes analysis regarding extreme conditions utilizing empirical and statistical models. Related modelling approaches were implemented and tested in the fire-enabled DGVM ORCHIDEE-SPITFIRE (chapter 4). New drivers of fire danger were evaluated in the Integrated System for Wildland Fires (IS4FIRES, chapter 5). And finally, to gain deeper insights in fuel characteristics regarding the species composition, the

representation of species reproduction success and subsequent species distribution was analyzed by the process-based Phenofit-SIERRA (chapter 6).

# 2 Using Machine Learning to analyze human-caused fires

## 2.1 Introduction

Up to now, fire-enabled DGVMs incorporated the human component of fire ignitions in a greatly simplified way. In the SPITFIRE models, the number of human-caused ignitions is modelled as a non-linear function of population density only (Thonicke et al., 2010). In order to get a more complete picture about the relationship between human factors and fire ignition and to subsequently improve the SPITFIRE models, we applied machine learning techniques to several predictor variables and identified the most influential ones. The results were further used to derive more accurate functional relationships between the predictors and fire ignitions.

## 2.2 Data sets used

For the analysis, 10 human predictor variables were selected. These were compiled for three of the five regional pilot sites defined within the FirEUrisk framework (Central Europe, Barcelona and Central Portugal) which represent fire-prone regions of varying degrees of risk and which were readily provided by partners at the University of Lleída (UdL). The variables are described in Table 1. Population percentage over 65 was calculated from absolute population numbers (population over 65 / total population * 100). Fuel types were derived through reclassification of CORINE land cover data into 4 different classes (no fuel, grassland, shrubland, forest). Land cover interfaces were derived from the intersection of reclassified CORINE land cover data into the four classes wildland, urban, agricultural and grassland. Distances to these interfaces, as well as distances to roads were computed using the Euclidean distance. The coverage percentages were computed through a combination of area calculation, intersection, dissolve and statistical operations. All variables were resampled to a spatial resolution of 100x100 m and projected into the ETRS89-extended / LAEA Europe (Lambert Azimuthal Equal Area) coordinate reference system.
For the 3 pilot sites, fire records with ignition point data are available. It was compiled by local authorities and serves as the data source for the response variable in the machine learning model. Table 2 shows the temporal coverage and the size of the records. For the Central Europe region, four data records from different authorities were combined.
For the translation to the European scale, the predictor variables that were found to be most important in the model were later recompiled for all of Europe according to the described methods above and resampled onto the 9 km resolution grid used in the DGVMs.

*Table 1:Human predictor variables used for training the machine learning model*

| Variable | Source | Year | Unit |
|---|---|---|---|
| 1. Population density | SEDAC-CIESIN v4.11 | 2020 | ppl/km$^2$ |
| 2. Population older than 65 | EUROSTAT (LAU level) | 2011 | % |
| 3. Distance to roads | GRIP-GLOBIO (region 4) | 2018 | m |
| 4. Fuel types | CORINE Land Cover - Copernicus | 2018 | categorical |
| 5. Distance to wildland-urban interface | CORINE Land Cover - Copernicus | 2018 | m |
| 6. Distance to wildland-agricultural interface | CORINE Land Cover - Copernicus | 2018 | m |
| 7. Distance to wildland-grassland interface | CORINE Land Cover - Copernicus | 2018 | m |
| 8. Percentage urban land cover | CORINE Land Cover - Copernicus | 2018 | % |
| 9. Percentage agricultural land cover | CORINE Land Cover - Copernicus | 2018 | % |
| 10. Percentage wildland land cover | CORINE Land Cover - Copernicus | 2018 | % |

*Table 2: Fire records from 3 pilot sites used as response variable in the machine learning model*

| Site | Temporal coverage | Number of ignition points |
|---|---|---|
| Central Europe | 2008-2022 | 24,235 |
| Czech Republic | 2018-2020 | 5,741 |
| Poland | 2017-2022 | 17,036 |
| Germany (Brandenburg) | 2008-2021 | 516 |
| Germany (Saxony) | 2010-2020 | 942 |
| Barcelona | 2008-2018 | 2,462 |
| Portugal (north) | 2001-2015 | 11,111 |

## 2.3 Methods and predictor analysis

We employed a Random Forests (RF) classification model (Breiman, 2001) to derive variable importance and partial dependencies of fire ignition on each of the ten predictors. For this, the data from all three pilot sites was merged for all variables and a raster stack was created. Since the response variable is binary - either an ignition occurred or not - a random sample of pseudo-absence points (twice the amount of presence points) was created representing areas where no ignition happened. We extracted the predictor variable values at each of the point locations and compiled them into a data frame. We split the data into training data which served as input for the RF model (75%) and testing data used for validating the results (25%). The RF classification algorithm was then trained and validated 10 times using 5-fold cross-validation procedure. The parameters that were used for most models were mtry = 6 and ntree = 500. The model results were applied to the testing data and the area under the curve (AUC) value was recorded for each model. Finally, the model with the highest AUC was selected as the final model and variable importance was examined. For the most important variables, partial dependence plots (PDPs) were computed to examine the partial relationship between the predictor and the response variable.

In order to obtain functional relationships that can be described with simple equations, we made use of the SOFIA modelling approach (Forkel et al., 2017). This procedure was initially developed for estimating burned area but is used here for the estimation of ignition probability. It approximates the functional relationship between a predictor and a response variable by fitting a logistic function. We examined the PDPs of the most important predictors from the RF model to estimate priors for the logistic function. A GENOUD optimization algorithm (GENetic Optimization Using Derivatives) was then run to minimize the sum-of-squared error (SSE). The resulting optimized logistic functions of each predictor were then combined into a SOFIA model and used for the prediction of ignition probability on the pilot site scale and later also on the European scale. Confusion matrices and boxplots were created quantifying the prediction performance of the SOFIA model.

All computations were implemented using the programming language R (4.2.2). Primarily used libraries include raster (3.6.3) for handling raster data, randomForest (4.7.1) and caret (6.0.92) for implementing the RF algorithm, pdp (0.8.1) for deriving partial dependencies and creating plots and SOfireA (1.1) for implementing the SOFIA modelling approach.

## 2.4 Results (PS and ET, incl. plausibility check)

The best-performing RF model achieved an out-of-bag error of 18.71% and an AUC of 0.861. The confusion matrix revealed an F1 score of 0.868, a false positive rate of 21.0% and a false negative rate of 17.5% (Tab. 3).

The most important human predictor for fire ignition according to the RF model is population density, followed by distance to the wildland-grassland interface, population over 65 and distance to roads. The most irrelevant variables turned out to be fuel type and land cover percentage of the 3 main types (Tab. 4).

*Table 3: Confusion matrix for validation of RF model (0: non-ignition point, 1: ignition point)*

| | 0 | 1 |
|---|---|---|
| 0 | 9354 | 1979 |
| 1 | 878 | 3299 |

*Table 4: Variable importance of predictors in RF model*

| Importance rank | Predictor variable | %IncMSE |
|---|---|---|
| 1 | Population density | 283.77 |
| 2 | Distance to wildland-grassland interface | 231.92 |
| 3 | Population older than 65 | 224.95 |
| 4 | Distance to roads | 219.64 |
| 5 | Distance to wildland-agricultural interface | 178.86 |
| 6 | Distance to wildland-urban interface | 174.56 |
| 7 | Percentage agricultural land cover | 104.56 |
| 8 | Percentage wildland land cover | 92.42 |
| 9 | Percentage urban land cover | 81.50 |
| 10 | Fuel types | 45.88 |

For the SOFIA model, only the most important variables (see Fig. 1) were considered. From their PDPs parameters for a logistic curve fit were estimated. These served as priors for the GENOUD optimization algorithm. Following the optimization, it became apparent that for 3 of the 6 variables, no clear logistic relationship could be estimated (Fig. 2). The predictors distance to the wildland-grassland interface, population over 65 and distance to the wildland-agriculture interface were subsequently dismissed and the SOFIA model was configured and optimized again with the 3 remaining predictors population density, distance to roads and distance to the wildland-urban interface. The final curve fits are shown in Fig. 3.

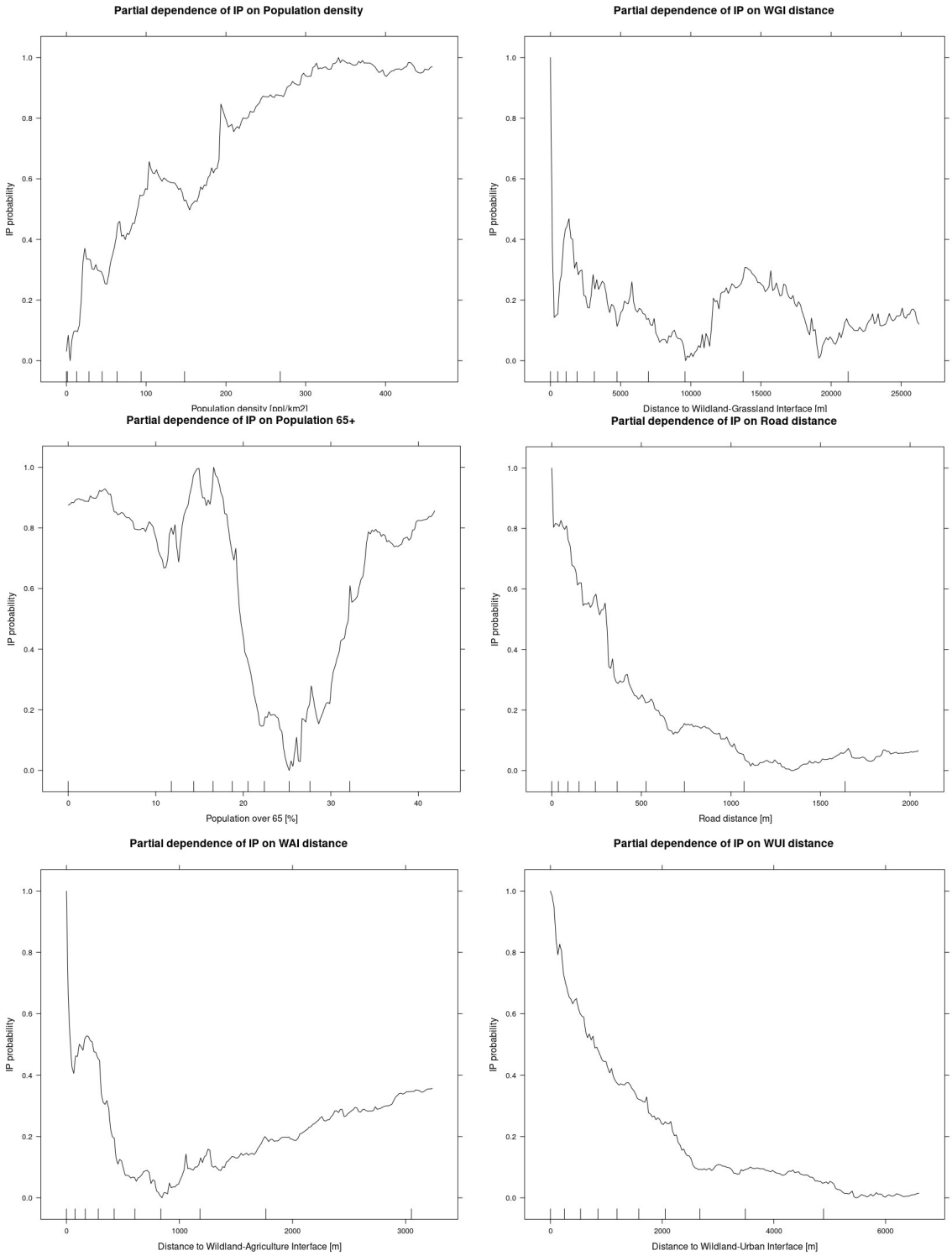


*Figure 1: Partial dependence plots for the six most important variables in the RF model*

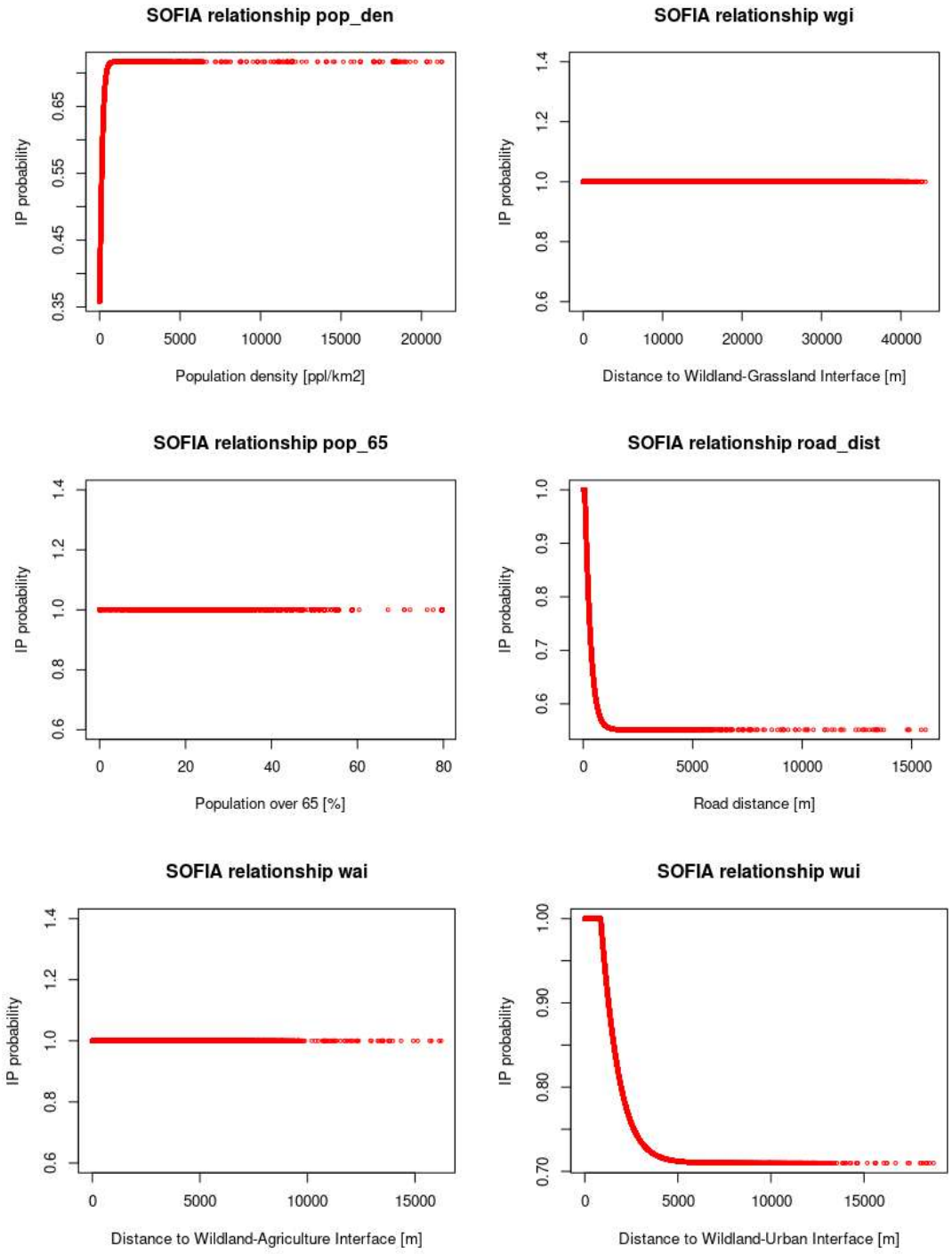


*Figure 2: Estimated functional relationships after optimization for the 6 most important variables from the RF model*

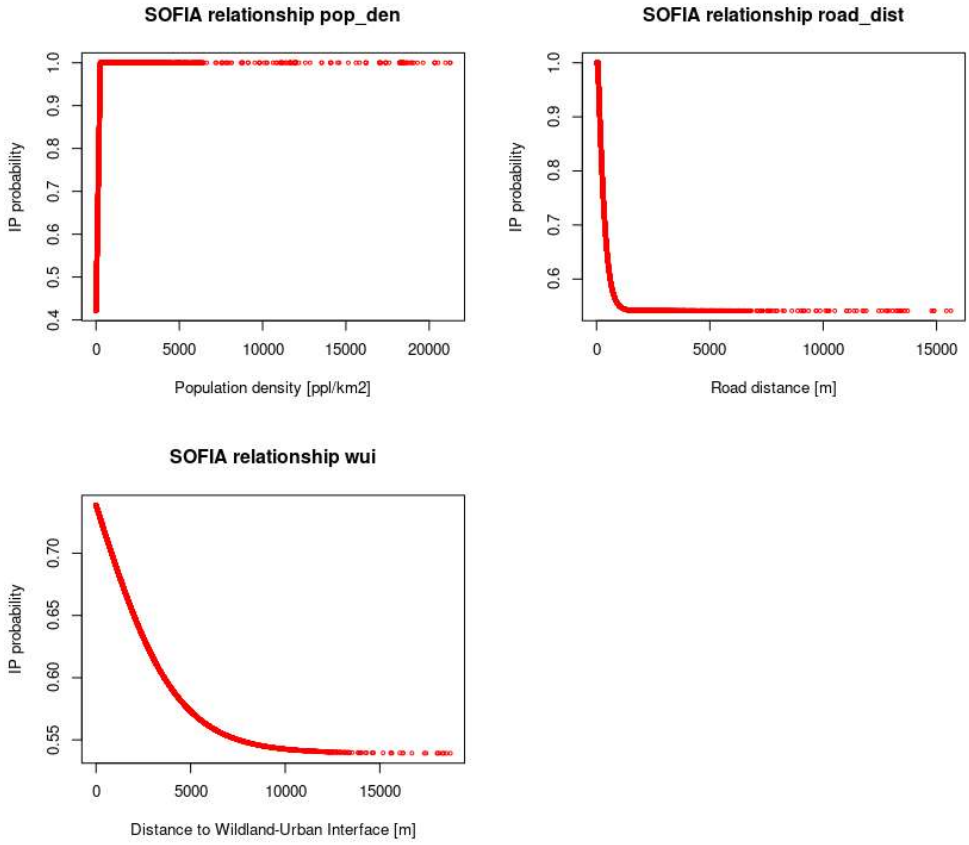


*Figure 3: Estimated functional relationships after optimization for the 3 remaining variables*

The identification of the most important human variables for predicting fire ignitions and their functional relationships with the response variable leads to the final equation of ignition probability being described as:

$$IP_{prob} = f(pop_{den}) * f(road_{dist}) * f(WUI_{dist})$$

Every single function in this product represents a logistic function with four parameters each in the format of:

$$f(x) = \frac{max - min}{1 + e^{-sl*(x-x_0)}} + min$$

with $min$ representing the lower asymptote, $max$ representing the upper asymptote, $sl$ representing the slope and $x_0$ representing the turning point. The parameters that were obtained for each predictor variable are shown in Tab. 5.

*Table 5: Parameters for the logistic function for the 3 predictors in the SOFIA model*

| Parameter | Population density | Distance to roads | Distance to wildland-urban interface |
|---|---|---|---|
| Min | -2.860257 | 0.541457 | 0.539226 |
| Max | 3.702918 | 1.603163 | 0.937873 |
| Sl | 1.359550e-03 | -4.705747e-03 | -4.759458e-04 |
| $x_0$ | 1.152925e-08 | -1.655536e-07 | -1.212866e-08 |

Using the obtained SOFIA function for predicting human ignition probability from the original data yields adequate results, as seen in the confusion matrix and the boxplot in Tab. 6 and Fig. 4. Naturally, the performance has slightly decreased with an F1 score of 0.776 and an AUC of 0.663. However, the percentage of false negatives has only marginally increased at 22.4%, while the percentage of false positives is now at 44.9%. The prediction results for each pilot site were also plotted (Fig. 5).

*Table 6: Confusion matrix for prediction of human ignition probability from final SOFIA model (0: non-ignition point, 1: ignition point)*

| | 0 | 1 |
|---|---|---|
| 0 | 24068 | 6950 |
| 1 | 6967 | 8542 |

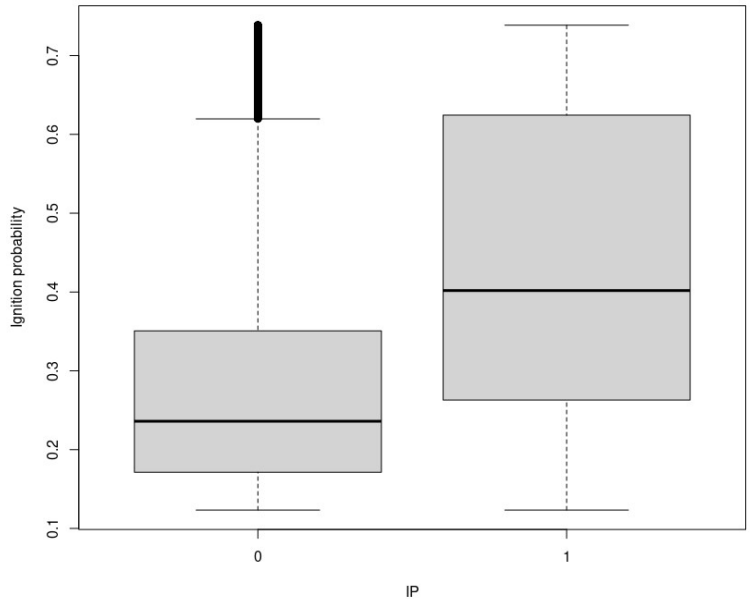


*Figure 4:Boxplot for prediction of human ignition probability from final SOFIA model (0: non-ignition point, 1: ignition point)*

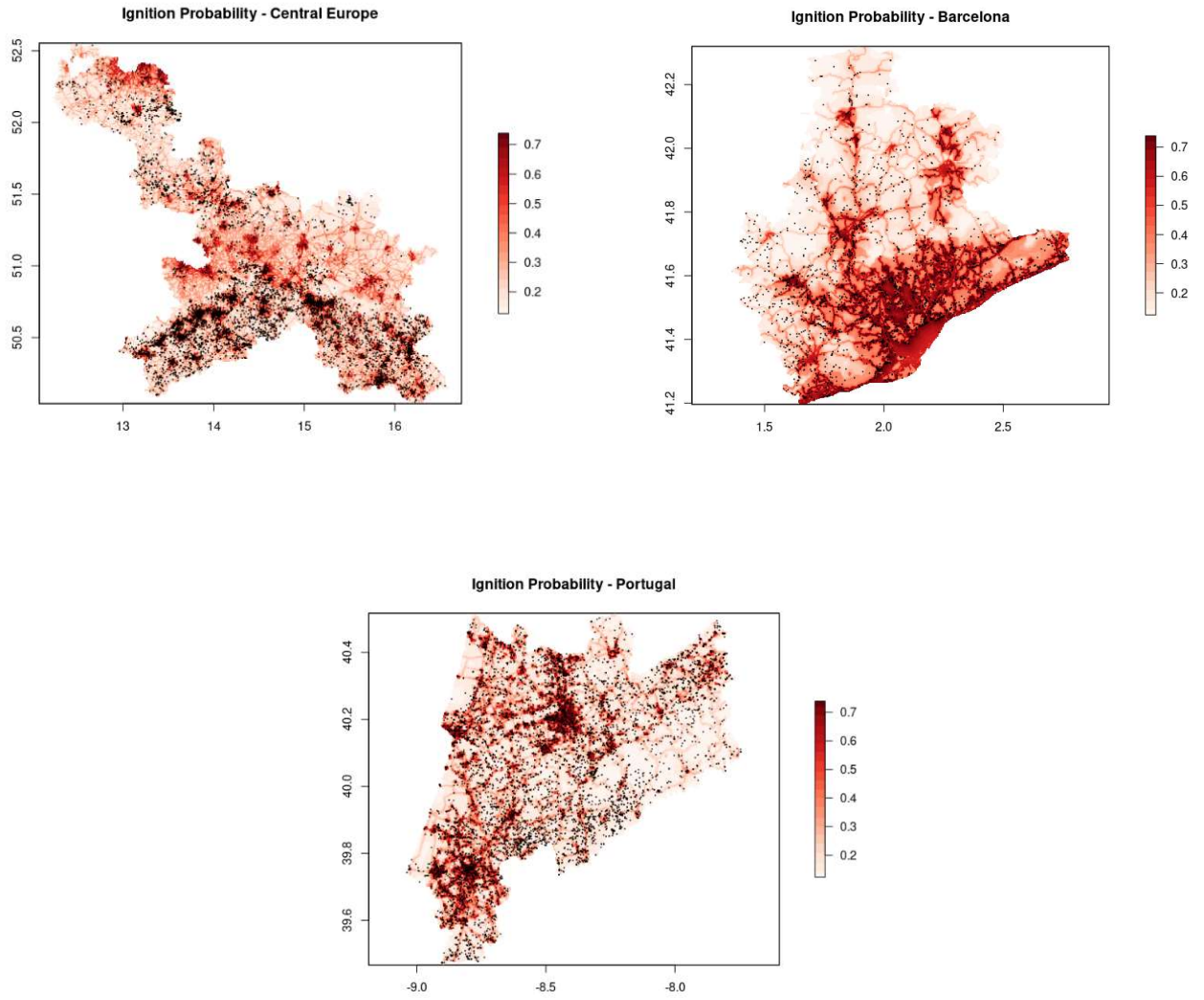


*Figure 5:Predicted human ignition probability from SOFIA model for all 3 pilot sites (black dots represent actual ignition points).*

Finally, the SOFIA function was used to predict ignition probability for the whole European territory. For this, the 3 required predictor variables were compiled for this scale according to the methods shown above, aggregated to the 9 km resolution used in the SPITFIRE module and cropped to the correct extent. The final probability map is shown in Fig. 6.

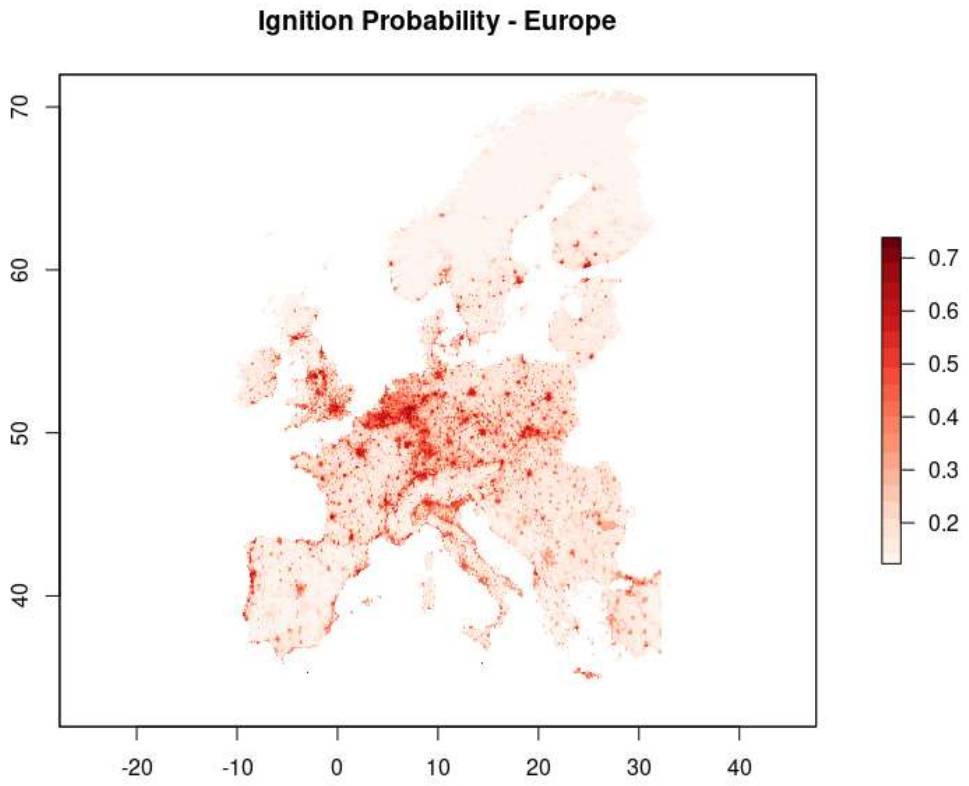


*Figure 6: Predicted human ignition probability from SOFIA model for the whole European territory*

## 2.5 Outlook

The map of human-caused ignition probability will be used as input to DGVMs in order to improve the modelling of fire ignitions. Furthermore, projections of population density, future spatial distributions of roads and the distance to the wildland urban interface can be used together with the approximated functions to calculate dynamic human ignition probabilities of the future.

# 3 Improving human ignitions in fire-enabled DGVMs

This chapter describes the improvements of individual fire-enabled dynamic global vegetation models (DGVMs) to allow the application of up-to-date model versions. For the deliverable D3.3 we focus on improvements in LPJmLv5.3-SPITFIRE, developed at PIK LPJ-GUESS-SPITFIRE, developed at SGN. Both models implemented and tested the hybrid function of human-caused ignition, developed in chapter 1.

## 3.1 LPJmLv5.3-SPITFIRE

### 3.1.1 Model Description

The Lund-Potsdam-Jena managed Land (LPJmL) model (Von Bloh et al., 2018) simulates both natural and agricultural ecosystems, as well as land-atmosphere exchange flows of carbon and water on a global scale. The model simulates vegetation dynamics on the basis of plant functional types (PFTs) including eight woody and three herbaceous PFTs (Schaphoff et al., 2018). Agriculture is based on eleven prescribed crop functional types including irrigation. Vegetation dynamics are driven by daily climate input data (temperature, precipitation and radiation), atmospheric $CO_2$ concentration, soil data and land-use management. To simulate wildfires interacting bidirectionally with vegetation dynamics, the DGVM is coupled to the Spread and InTensity of FIRE fire model "SPITFIRE" (Thonicke et al., 2010). The coupled model LPJmL-SPITFIRE operates on daily timesteps and varying spatial resolution depending on the climate and soil input data.

SPITFIRE simulates the ignition and spread of wildfires on a global scale. In this process-based model, wildfires originate from potential human ignitions and lightning-caused ignitions, from which an internally calculated fire danger index (vapour pressure deficit or Nesterov index) predicts the proportion of ignition events turning into spreading fires. The resulting fire spread is calculated on the basis of the Rothermel equation (Rothermel, 1972), which depends on wind speed, fire intensity, and the availability, composition and wetness of the fuel. Fire durations in the original SPITFIRE version are limited to 240 min following the assumption that larger fires and multi-day burning can be replaced by a number of smaller fires igniting each day independently. Overall, simulated fire regimes in LPJmL-SPITFIRE depend on an interplay of potential ignitions, fire weather and fuel loads (Thonicke et al., 2010). The SPITFIRE model was updated by Drüke et al. (2019) where the Nesterov Index was replaced by an index based on vapour pressure deficit, and a parameter optimization was conducted to improve the interannual variability of burned area (Drüke et al., 2019).

### 3.1.2 New model improvements with hybrid functions

**General model improvements**

To improve model performance and reduce uncertainties of simulated wildfires, the following new processes and adaptations have been implemented into the LPJmL-SPITFIRE model.

Fuel load and composition used by SPITFIRE are directly simulated by the LPJmL vegetation modules. Improving the simulated vegetation, accordingly enhances the modelling quality of fuels used by SPITFIRE. We therefore coupled SPITFIRE to the latest version of LPJmL5.3 (Von Bloh et al., 2018), which now includes nitrogen limitation of the dynamic vegetation where nutrients can enhance (reduce) vegetation productivity, thus production and composition of dead

fuel. Furthermore, LPJmLv5.3 now allows the computation of dead fuel moisture directly from the litter layer (Lutz et al., 2019). This improved the representation of fuel load and composition and fuel wetness in our model.
In addition, multi-day burning was implemented and now allows extended fire durations. Comparing simulated fire duration against observations had shown that SPITFIRE underestimates this variable while simulating burned area in reasonable dimensions. To overcome this discrepancy, the implemented multi-day burning approach now shows improved fire ignition distribution and burned area for more realistic reasons. In addition, the original standard SPITFIRE version generally overestimated ignitions, in order to compensate for shorter fire durations. Implementing longer and more realistic fire durations, model ignitions could be generally reduced. In our multi-day burning approach, individual fires continue to burn until the model internal fire danger index drops below 0.5% or up to 7 days maximum. Maximum daily fire duration was increased from 4h to 8h. Moreover, we now allowed wildfires to burn on managed grasslands (rangeland and pastures as denoted in Deliverable 3.2).

**Improvements of human ignitions with hybrid functions**

In the original SPITFIRE version, potential human ignitions only depend on an empirical inverted u-shaped relation to local population density (Thonicke et al., 2010). However, recent studies have shown (Moreira et al., 2011; Forkel et al., 2017) human caused ignitions also depend on other socio-economical or landscape related variables such as GDP or distance to wildland-urban interfaces. This is particularly important in an area as highly characterized by cultural landscapes such as Europe. Therefore, we replaced the original calculation of potential human ignitions with the more complex SOFIA hybrid function approach (see chapter 1) and compared simulations of this alternative forcing with simulations using human ignitions from the original SPITFIRE version. Potential human ignitions from the SOFIA approach (SOFIA ignitions thereafter) were based on the ignition probability map provided by TUD (see chapter 1). To translate the ignition probability into potential human ignitions, we scaled the SOFIA ignition probability with the same factor for all grid cells. This scaling factor could not be calculated directly, because ignition points used to create the ignitions probability map stem from different time periods. Hence, we set the scaling factor, so that the maximum of the resulting potential SOFIA ignitions match with the maximum potential human ignitions from standard SPITFIRE (Fig. 7).

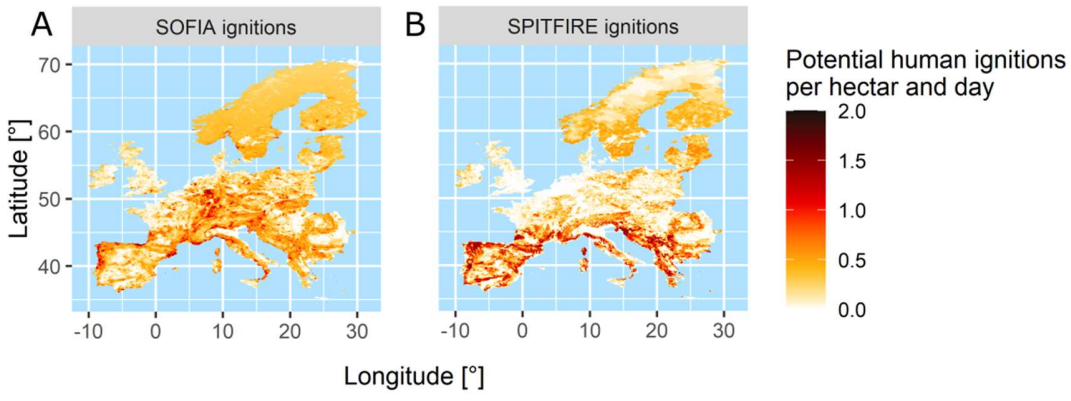


*Figure 7: Comparison of potential human ignitions in the SOFIA modelling approach (Panel A) and standard SPITFIRE (Panel B). Potential human ignitions were less pronounced in Southern Europe (<45°N) using the SOFIA approach*

*compared to standard SPITFIRE. Potential human ignitions are higher and more homogeneously spread in central Europe and Scandinavia using the SOFIA based approach implemented in LPJmL-SPITFIRE.*

Finally, to explore the improved LPJmL5.3-SPITFIRE model, including land-use and the improvements described above (Drüke et al., 2019; Lutz et al., 2019; Thonicke et al., 2010; Von Bloh et al., 2018), we applied it to the European Scale (ET) using a 9km grid cell resolution. For manually tuning the PFT-specific parameters for the VPD based fire danger index from Drüke et al. 2019, we run simulations using climate input data from WFDE5 on a 0.5 x 0.5 grid resolution (Cucchi et al., 2020), so that simulated patterns of burnt ensemble validation data from GFED4s. Final model simulations were forced by provided downscaled bias-corrected climate input from Task 3.1.1 (D3.1) from five different General Circulation Models (GCMs: ACCESS-CM2, CanESM5, CMCC-ESM2, CNRM-ESM2-1, EC-EARTH3, temporal coverage: 1950 - 2014) and historical land-use data from Task 3.1.2 (D3.2). For each GCM, we started the model simulation from the bare-ground and recycled the first 30 years of the input climate data (1950-1979) for a total period of 10,000 years bringing the simulated vegetation into equilibrium (natural vegetation spin-up phase, without any human activity). Thereafter, we performed a subsequent spin-up of 390 years including land-use, followed by the final transient simulations from 1950 to 2014 (also incl. land-use). Population density and potential human ignitions were held constant for the land-use spin-up and the subsequent transient run.
We conducted this simulation experiment with the two different ignition approaches: human ignitions as implemented in the original SPITFIRE version and the alternative SOFIA based ignitions. We compared the last 10 years of simulated burnt areas (2003 to 2014) of both ignition approaches with a satellite-based product from GFED4s (Randerson et al., 2017).

### 3.1.3 Results and Discussion

Our results show that the burnt area simulated by LPJmL5.3-SPITFIRE agrees well to observations from GFED4s (Fig. 8 and Fig. 9). Annual burnt area from GFED4s mostly lies within the envelope of the ensemble run across all GCMs for both ignition setups (Fig. 8).
Spatial patterns of simulated burnt area well agree for south-eastern Europe with GFED4s (Fig. 9). In other parts of Southern Europe, we found slight differences in Italy and on the Iberian Peninsula. In central Europe, simulated fire activity is higher in western Europe compared to central Europe, which matches the validation data. Simulated burnt area is currently lower in north-eastern Europe compared to GFED4s, which could also not be improved through the new ignition approach (SOFIA ignitions).
Including the new ignition approach in our simulations decreased the squared error of the simulated burnt area in central Spain, northern Portugal and parts of south-eastern Europe (Fig. 10, Panel C), which indicates increasing model performance in those areas. In southern France integrating the new potential human ignitions increased simulated burnt area and therefore a higher deviation from GFED4s.

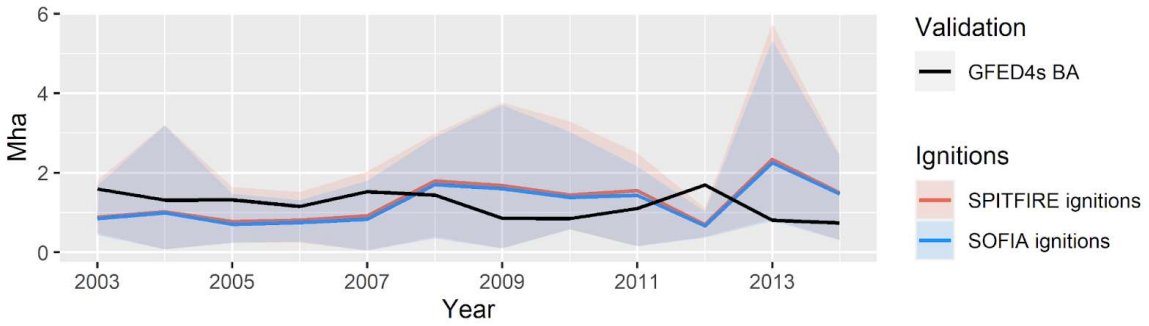


*Figure 8: Mean annual burnt area [Mha] of the last 10 years (2003-14) of the simulation period for both ignition approaches (standard SPITFIRE ignitions: red line; SOFIA ignitions implemented in LPJmL-SPITFIRE: blue line) compared to GFED4s (black). Envelopes show the minimum and maximum of the ensemble runs of all GCMs.*

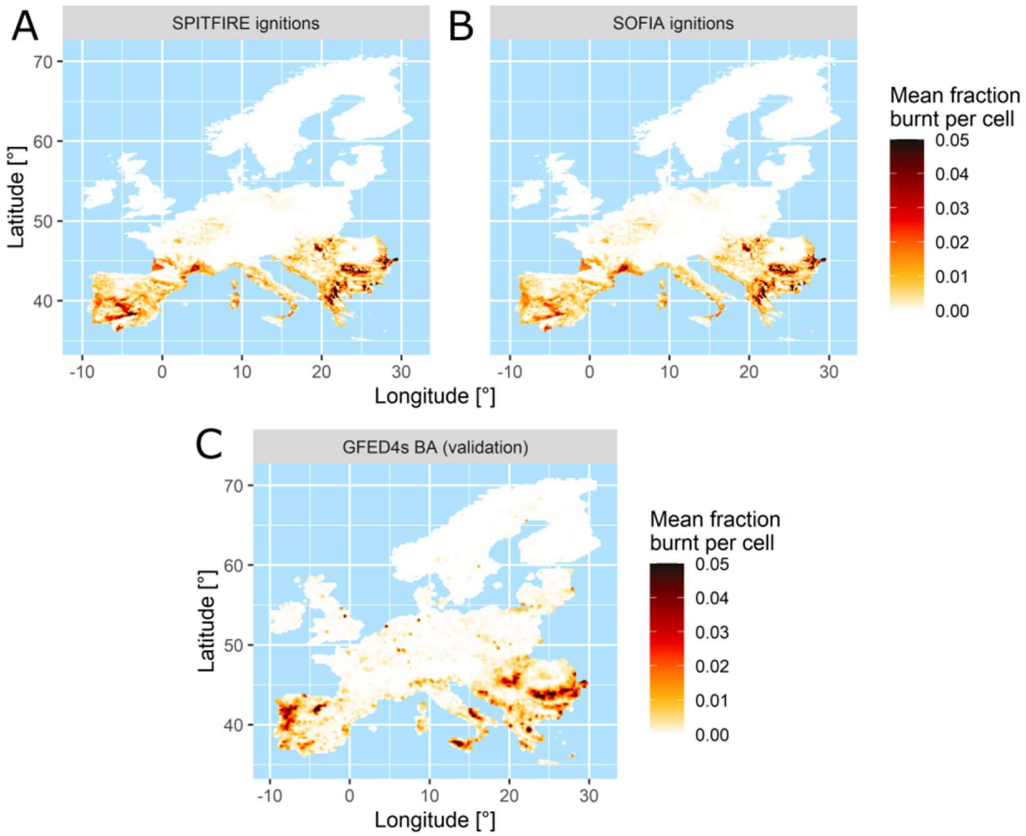


*Figure 9: Averaged burnt area between 2003 and 2014 across all GCMs from standard LPJmL5.3-SPITFIRE (panel A), the SOFIA approach implemented in LPJmL-SPITFIRE (Panel B) and satellite-based observations from GFED4s (Panel C).*

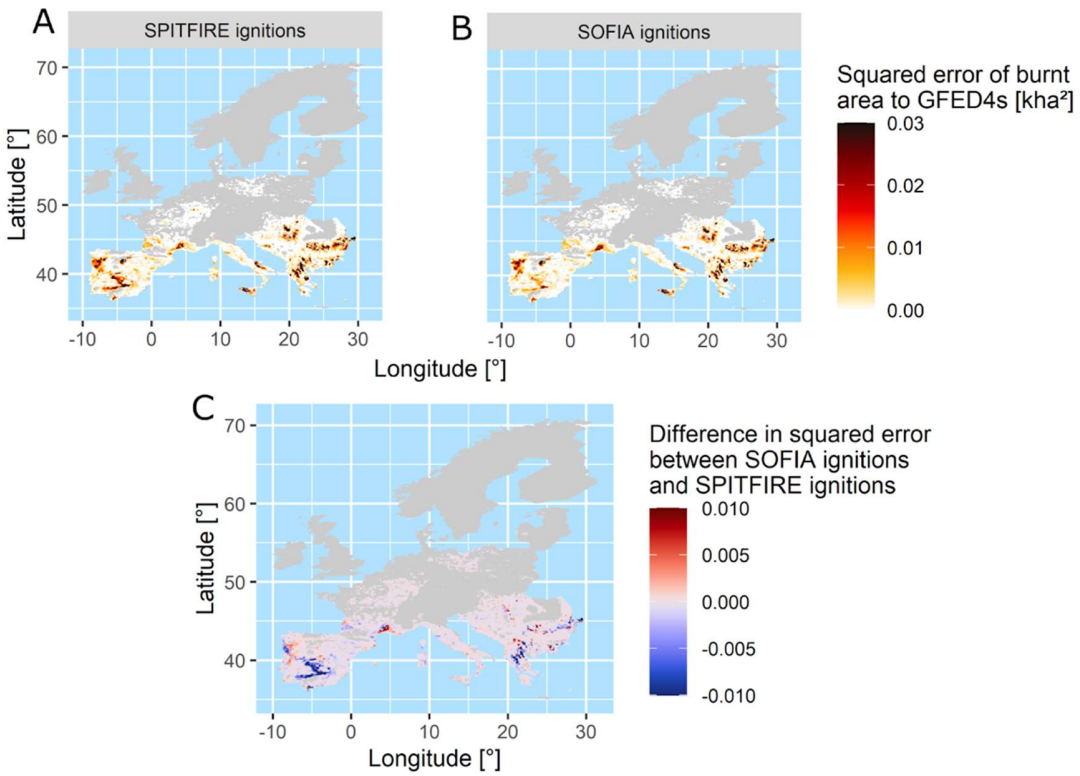


*Figure 10: Squared error (squared difference between simulation and validation) of simulated burnt area for SPITFIRE ignitions (Panel A) and SOFIA ignitions implemented in LPJmL-SPITFIRE (Panel B) to GFED4s. Panel C shows the difference squared error between both model runs (difference between Panel A and Panel B): Negative values (blue colours) indicate model improvement and positive values (red colours) higher deviation from GFED4s. Areas where the mean simulated burnt area was smaller than 1ha were masked out in grey. Squared errors > 0.01 indicate areas, where simulations differ more than 100ha from GFED4s.*

In general, our results show that LPJmL5.3-SPITFIRE agrees well with the remote sensing data from GFED4s. Differences in annual variability from the validation data might originate from the poor representation and prediction of extreme drought events in CMIP6 models (Scoccimarro & Navarra, 2022). In addition, different interannual variability among the GCMs causes asynchronous or synchronous concurrence of wet and dry years within the GCM ensemble. This explains the large variability of the GCM envelope of the simulated burnt area in Fig. 8. If model simulations were driven by historical reanalysis data, errors in simulated burnt areas might be lower. Nevertheless, mean simulated observed annual burnt area (Fig. 8, colored lines) is well in range of GFED4s (Fig. 8, black line) and spatial patterns are similar between model simulation and GFED4s. Altogether, this indicates that LPJmL5.3-SPITFIRE is capable of adequately simulating wildfires on the European scale.

Regarding the new ignition approach, we found that using SOFIA ignitions leads to a model improvement in Southern European regions such as central Spain, northern Portugal and parts of south-eastern Europe. Indicating that the new ignitions especially improve model performance in fire prone areas. Surprisingly, simulated fire activity using the new

ignition approach is rather similar in most other regions (see differences between SPITFIRE and SOFIA ignitions in annual burnt area, Fig. 8, spatial distributions, Fig. 9), which underlines the robustness of both ignition approaches on the larger European scale. Yet, potential human ignitions in the new approach now depend on three different variables (see chapter 1) instead of one (population density in standard SPITFIRE). Therefore, we expect a better representation of ignitions for future fire risk simulations using the new ignition approach based on the SOFIA model.

### 3.1.4 Outlook

In the next steps, we will conduct the simulations of future fire regimes including the improvements described above and using the new SOFIA approach for potential human ignitions. We expect changes in potential ignitions and burnt area as a result of changes in human population density and changes in land-use. Additionally, climate change affects fire danger and plant productivity, which could in turn increase or decrease burned areas. The net effect of land-use change and climate change is still unknown, because future land-use change might counterbalance climate change effects where landscape fragmentation decreases due to land abandonment, or reduced vegetation productivity increasingly limits fuel load.

Finally, we found that further parts of the model could be improved. For instance, we detected that parts of the Rothermel equation were insufficiently implemented in the standard SPITFIRE version. In addition, LPJmL5.3-SPITFIRE currently simulates unphysically low live grass moisture, which might lead to an unrealistic strong fire spread in grasslands in the current version. Therefore, we seek to further improve LPJmL5.3-SPITFIRE in our upcoming work.

## 3.2 LPJ-GUESS

### 3.2.1 Model Description

LPJ-GUESS is a process-based dynamic vegetation-terrestrial ecosystem model designed for regional or global studies. The model integrates eco-physiological processes, such as photosynthesis, autotrophic and heterotrophic respiration, and plant growth with individual-based tree population dynamics and biome biogeography (Smith, Prentice, & Sykes, 2001; Smith et al., 2014). Based on environmental input data, such as climate, soil and atmospheric composition, the detailed representation of vegetation dynamics enables insights in local forest ecosystem composition as well as large scale spatial trends of vegetation - bridging the gap from stand level to continental scale. A detailed description of LPJ-GUESS is available in Smith et al. (2001) and Smith et al. (2014).

Similar to LPJmL5.3 in 3.1, the DGVM is coupled to the Spread and InTensity of FIRE (SPITFIRE) fire model (Thonicke et al., 2010) which enables simulations of fire regimes and the impact of fire on the terrestrial carbon cycle and associated emissions of trace atmospheric constituents. The process-based fire model explicitly considers fuel characteristics by combining environmental fire drivers, such as wind and topography, and linking vegetation traits to fuel class characteristics (fuel classes are live grass and dead 1hr, 10hr, 100hr fuels). Simulated fire processes consider potential human and lightning hazards which, under suitable climatic and vegetative conditions, lead to actual ignition events shown by a number of fires in each grid cell. The severity of those fires is reflected by the Rothermels fire spread rate and can intensify by environmental conditions such as high winds. As a result of fire, mortality takes place and stored vegetation carbon is released into the atmosphere. In summary, LPJ-GUESS-SPITFIRE complements the feedback loop

from vegetation dynamics on fire events and vice versa. As the final model setup considers complex plant interactions and high-resolution data, demonstrated results are limited to the Demonstration areas and pilot sites of the FirEUrisk project only. Comprehensive simulations of the entire European domain under different climate scenarios will be carried out as part of the next deliverable (D3.4).

### 3.2.2 Model setup and the two tested human ignition approaches

Simulations describe the FirEUrisk Demonstration Areas and pilot sites across Europe. The parameters of the model reflect global plant functional types (PFTs) representing trees, shrubs and grasses. Climate forcing was based on downscaled bias-corrected historical data (~200,000 grid cells at a 9km resolution, ACCESS-CM2 model, provided by deliverable D3.1., METEOGRID). The dataset includes daily maximum and minimum air temperature, precipitation, wind, and maximum and minimum relative humidity. Daily mean air temperature and daily mean relative humidity were approximated by maximum and minimum average. While fire processes in LPJ-GUESS-SPITFIRE are simulated daily, vegetation dynamics are updated annually. In total we simulated a timeframe from 1450-2014, starting from bare ground in every grid cell. In order to investigate the vegetation at equilibrium we simulated 500 years of spin-up (cycling climate from 1950-1971), before the investigated 65 year period from 1950 to 2014. Atmospheric CO2 concentrations were assumed transient over time (Quéré et al. 2018). Soil conditions were calculated by constant fractions of sand, soil and clay. Slope was not considered. The model was run without land use, i.e. the potential natural vegetation was simulated.

So far, potential human ignitions of LPJ-GUESS-SPITFIRE have considered population density only (approach by original SPITFIRE version (Thonicke et al., 2010)). There, the original human-caused ignitions are modelled as a non-linear function $HI(P_D)$ that increases with population density $P_D$ in rural areas but decreases with $P_D$ in densely populated urban areas (Thonicke et al., 2010). The function further comprises a site-specific factor $a$ that reflects the propensity of people to produce ignition events.

$$HI(P_D) = P_D * 30 * e^{-0.5*\sqrt{P_D}} * a$$

In the newly implemented approach, we replaced the original calculation of potential human ignitions with the more complex SOFIA hybrid function of chapter 1. Potential human ignitions are calculated within the model for each grid cell based on the parameters from the SOFIA approach and input data of population density $P_D$, wildland-urban-interface distance $WUI_D$ and distance to roads $R_D$ given as input variables. To predict the number of fires related to the ignition probability we assumed a scaling factor $k = 0.0115/365$ (similar to LPJmL-SPITFIRE).

$$HI(P_D, WUI_D, R_D) = f_{ML}(P_D) * f_{ML}(WUI_D) * f_{ML}(R_D) * k$$

### 3.2.3 Results and Discussion

The two compared approaches that approximate the potential human ignitions show clear differences in their spatial patterns (Fig. 11). Particularly noticeable dissimilarities can be found in the southern demonstration areas (e.g. southern France, Spain) where the potential human ignitions of the original SPITFIRE approach are in general higher, except in urban areas. There, the difference between the two methods also become clearer. While the SPITFIRE approach has very low potential ignitions in densely populated areas such as Toulouse, Bordeaux and Barcelona, these are in contrast pronounced in the SOFIA approach. The reason for this is the monotonically increasing logistic function of population density in the SOFIA approach, which dominates in urban areas. Northern demonstration areas overall increase in potential human ignitions with the new approach. Again, urban areas such as Dresden show pronounced differences.

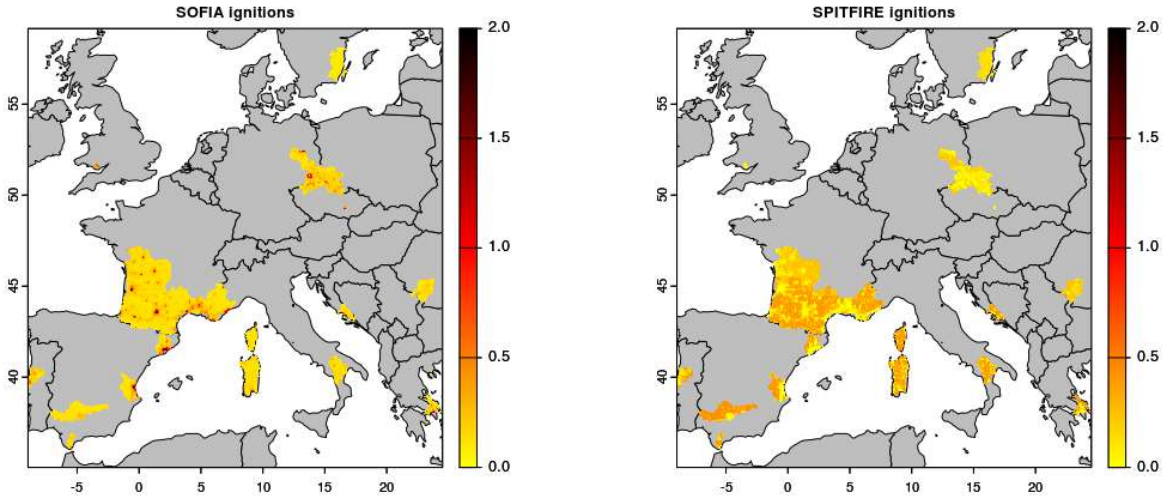


*Figure 11: Comparison of potential human ignitions in the SOFIA modelling approach (left) and standard SPITFIRE (right). Potential human ignitions were less pronounced in the Southern Demonstration Areas (e.g. Southern France, Barcelona Province, Croatia) using the SOFIA approach compared to standard SPITFIRE.*

With respect to burnt area, the differences are most significant in the southern regions, where potential ignitions are more likely to cause actual fires (Fig. 12). Here, the SOFIA approach predicts a lower burnt area than the original approach (for instance DAs in Spain). This is consistent with the LPJmL5.3-SPITFIRE comparison from the previous section. However, here we simulated much more severe fires, as the landscapes are fully covered with potential natural vegetation.

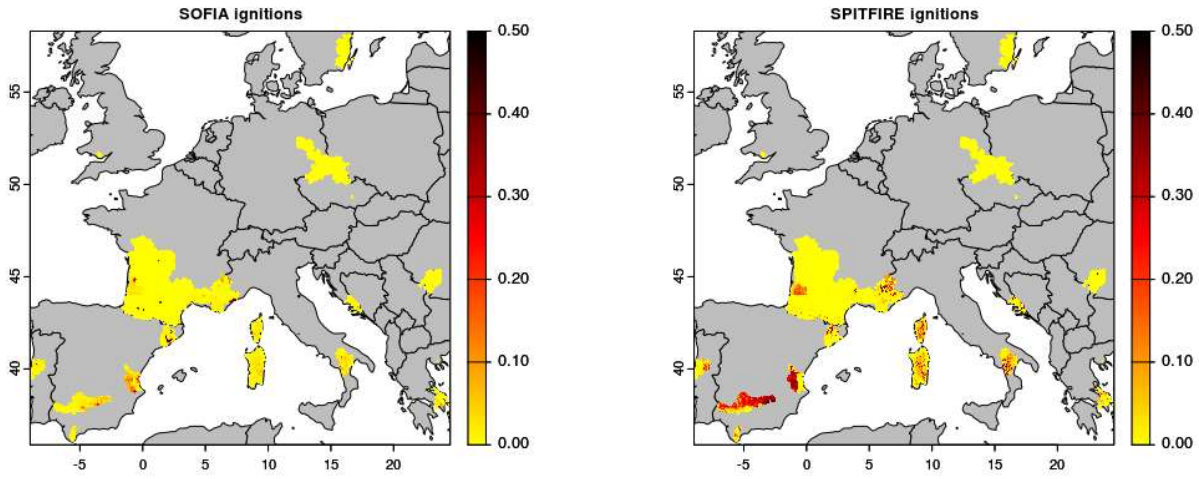


*Figure 12: Averaged annual burnt area between 1950 and 2014 based on standard LPJ-GUESS-SPITFIRE (right) and the SOFIA approach implemented in LPJ-GUESS-SPITFIRE (left).*

### 3.2.4 Outlook

In general, our findings are in line with the systematic analysis carried out with LPJmLv5.3-SPITFIRE. However so far, our simulations reflect a potentially natural vegetation (without land-use and management) and thus also potentially vegetated burning landscapes. Higher fractions of burned area imply the importance of fire suppression by landscape conversion. Historical land use data and future realizations (currently produced in Task 3.1) can help to gain a deeper understanding of fire severity with and without fuel management.

The explicit calculation within the LPJ-GUESS-SPITFIRE(-SOFIA) model enables analyses for dynamic human-induced conditions, for instance to investigate fire regimes under decreasing wildland-urban distances and increasing population densities that can be expected in the future. With more systematic investigations, these findings could serve as a basis for land management under socio-economical aspects.

# 4 Improving extreme fires in fire-enabled DGVMs

### 4.1.1 Model Description (ORCHIDEE)

The model being developed for this exercise is a widely used sub-branch of the land surface component of the IPSL Earth System Model, ORCHIDEE-MICT revision number 5308. This sub-branch of the overall ORCHIDEE model family is global in scope but includes some soil, hydrological and thermal processes specific to boreal and permafrost-affected

regions (Guimberteau et al., 2018; Zhu et al., 2015, 2016), whose development here with respect to fire serves to facilitate future developments to target fire impacts on soil thermal state as well as subsequent microbial respiration. At the core of the model is terrestrial biomass fixed by photosynthetic carbon (C) uptake, performed by 13 plant functional types (PFTs) with distinct primary production, senescence and carbon dynamics (Krinner et al., 2005). These include two crop, two grass and nine tree PFTs. The type and distribution of vegetation biomass synthesised can either be imposed on the model by inputting monthly or annual vegetation maps, or projected autonomously by the in-built dynamic global vegetation model (DGVM). Fixed biomass C is allocated to foliage, fruit, roots, above/below -ground sap, heart wood and carbon reserves which are transferred to two reactivity-differentiated litter pools. ORCHIDEE-MICT is integrated with a model-specific version (see Yue et al. 2014, 2015a) of the SPITFIRE fire module (Thonicke et al., 2010; Yue et al., 2014, 2015b), which takes the aboveground portion of these biomass components and allocates them to potential fire fuel classes differentiated by their potential time to combustion/oxidation. ORCHIDEE-MICT-SPITFIRE has been involved in multiple phases of the fire model inter-comparison project (FireMIP) (Hantson et al., 2016) and its predictions found to be within the range of those from available fire models (Forkel et al., 2019; Hantson et al., 2020; Li et al., 2019; Van Marle et al., 2017). Fire ignitions are controlled by lightning strikes and human ignitions, the latter of which is determined as a positive logistic function of population density. Vegetation flammability is determined by fuel and climatic conditions (Nesterov Index and Fire Danger Index). Burned area is controlled by fire spread rate and fire duration, as influenced by vegetation flammability, and affects fire $CO_2$ emissions. In addition, this model incorporates explicit riverine and floodplain dynamics, grassland management, grazing, wood harvest, and crop harvest modules, all of which may have direct cause-effect relationships with fire phenomena, and the package may in principal be run with the full earth system model (including dynamic atmosphere and oceans). ORCHIDEE-MICT can be run at up to a 0.25 degree resolution, although generally runs are performed with 0.5 or 1 degree grids to facilitate faster simulation runtimes on HPC clusters, and output can be returned at daily, monthly or annual resolutions. ORCHIDEE is coded in the FORTRAN 90 programming language.

### 4.1.2 New model improvements with hybrid functions

We aim to identify problems with the existing model which could prove highly consequential with respect to using the model for performing future projections: these were extreme fires, landscape fragmentation, and their interaction. Both are expected to increase into the future at global scale. Extreme fires will likely increase in frequency in Mediterranean, temperate and boreal regions of Europe, which itself contains some of the world's most fragmented landscapes. To our knowledge, no fire-enabled, earth system model-integrated land surface models have successfully attempted to represent these crucial elements of fire and landscape-fire phenomena into global fire models, with the potential to substantially bias representation of future fires in Europe and beyond. These are expanded upon below.

**Problem 1a: No extreme forest/crown fires represented**

**Introduction:** Extreme fires that spread through tree crowns are best typified by their substantially increased rate of spread once fire intensity and flame height are sufficient for combustion to occur and be sustained in the canopy. While this is the condition for crown fires to occur, once in effect their dynamics are best typified and hence represented by their rate of spread (ROS), which may be many times faster than that of ground fires. Modelling crown fire ROS was attempted in a land surface model by Ward et al. (2018), who based their crown fire ROS highly simplistically, by applying a fixed multiplication factor (3.34) to ROS for any fire in which the flame height exceeds canopy height, and

weighting the overall grid ROS to the fraction of the canopy for which this was the case, given vegetation cover and the fraction of area affected by high flame heights. The 3.34 factor was taken directly from Rothermel (Rothermel, 1991), which was itself based on observations from the northern Rocky Mountains, and not adapted, and this was then applied to the same ROS function used in the original SPITFIRE model (Thonicke et al., 2010):

$$ROS = (ROS * (1 - ck)) + ((ROS * 3.34) * ck) \quad \textbf{(1)}$$

Where ROS is the grid-scale average ROS, and ck the proportion of the canopy in the grid cell affected by flame scorch and hence subject to potential crown fire spread. This approach resuits in three issues: 1) Overestimation of crown fires extent and severity in N. Eurasia & Scandinavia; 2) Excess fires in boreal regions in general; 3) A single ROS factor necessarily lacks dynamism and differentiation between fire causes and effects; 4) Their simulations could not replicate the observed disparity in area-specific crown fire frequency between boreal Eurasia and N. America: Rogers et al. (2015) showed that forest fire intensity in boreal N. America was on average 35% higher than that in Eurasia, as measured by satellite-derived fire radiative power estimates.

Cruz et al. (2005) showed that fitted a crown fire ROS model based on observed Canadian data from mostly boreal forest regions (jack pine, red pine, black spruce). This yielded an optimum crown fire ROS model with the following form:

$$ROS_{crown} = \beta_1 * U_{10}^{\beta 2} * CBD^{\beta 3} * e^{(-\beta 4 * EFFM)}, U_{10} > 0 \quad \textbf{(2)}$$

Where $ROS_{crown}$ is crown fire ROS; $\beta 1 - 4$ are observationally determined parameters relating to wind speed ($U_{10}$), canopy bulk density (CBD) and estimated fine fuel moisture (EFFM). This model was shown to substantially improve prediction of crown fire ROS over the original Rothermel (1991) equations, however canopy bulk density is not output in ORCHIDEE-SPITFIRE.

**Solution:** A hybrid approach of these two methods was adopted for representing crown fire ROS and making it dynamic with windspeed. Variation in crown fire ROS in the Rothermel (1991) experimental fires ranges 5-10 – fold. 20ft windspeed in the original Rothermel (1991) paper varies from 16-96.5km/h; if we apply the 0.4 surface roughness correction factor to this it becomes 6.4-38.6 km/h, the same as the range applied in the calculation of model coefficients in Cruz et al. (2005). Thus modulation of $ROS_{Crown}$ will revolve around the central value of the variation observed in these studies (i.e. ((38.6-6.4)/2)+6.4)=22.5). The +/- variation=38.6-6.4)/2=16.1. We can modulate the 3.34 constant proposed by Ward et al. (2018) for ROS manipulation by the wind speed formulation, whereby gamma=3.34 is the central value, +/-1.872 = range(1.468-5.212).

We can express ROS in a given grid cell as:

$$ROS = (ROS * (1 - ck)) + ((ROS * 3.34) * ck) \quad \textbf{(3)}$$

Where:

$\alpha_{ROSfactor}$=+/- 1.872

$U_{model}$=$U_{10}$*0.4

$U_{mid}$=22.5

$$(ROS_{factor} = (U_{model} - U_{mid})/16.1) * \alpha_{ROSfactor} \quad \textbf{(4)}$$

Crown fires are thus simulated by subjecting changes to the (grid-scale) rate of spread through the proportion of a grid cell in which flame height is calculated to reach the crown by an observationally determined parameter that is itself scaled by windspeed in a range of variation given by observation –based numerical modelling. In ORCHIDEE, this is done

in a two-fold loop, where in a given timestep the fuel, fire danger, ignition and spread are calculated to acquire the flame height and crown scorch factors. These are saved and everything else reset to zero. The two variables and climatological windspeed are plugged into the Equation 4 in the second call option included in the rate of spread subroutine, and the whole code sequence is run again and crown fire ROS determined.

**Result:** Reasonable spatial distribution of crown fire –induced BA increases in some areas, but **increases too large** (BA=+10%, ECO2=+35%) and some regions counterfactual (e.g. some areas in boreal, steppe and temperate Eurasia): See Results section.

**Problem 1b: No representation of ecological traits that define responses to fire and combustion phenomena, difficult to expand model vegetation types for this purpose.**

**Introduction:** We hypothesised that the misrepresentation and over-estimation of crown fire extent in boreal Eurasia in the solution proposed to Problem 1 was due to the lack of species-specificity in ORCHIDEE, such that the PFTs representing boreal forest functional types may functionally represent photosynthesis and growth satisfactorily, but were necessarily unable to distinguish the different strategies for fire coping, which are strikingly different in boreal Eurasia (BOEU) versus N. America (BONA). The former tend to be characterized by more frequent, slow burning, low intensity ground fires; the latter by less frequent yet high intensity crown fires. These reflect different ecological and evolutionary strategies, whereby e.g. some N. American species are fire 'encouragers', using fire to their ecological advantage by accentuating the landscape and biome-scale effects of fire with one eye on gaining successional advantage over other species, whereas many species e.g. larch in boreal Eurasia are fire 'resisters', whose phenotypic traits are not geared towards supporting large-scale ground fires (see Rogers et al. 2015). However, although the ecological diversity of boreal forest species is low, it is would be both highly time-consuming and complex to attempt creation of several additional boreal PFTs specifically for this purpose.

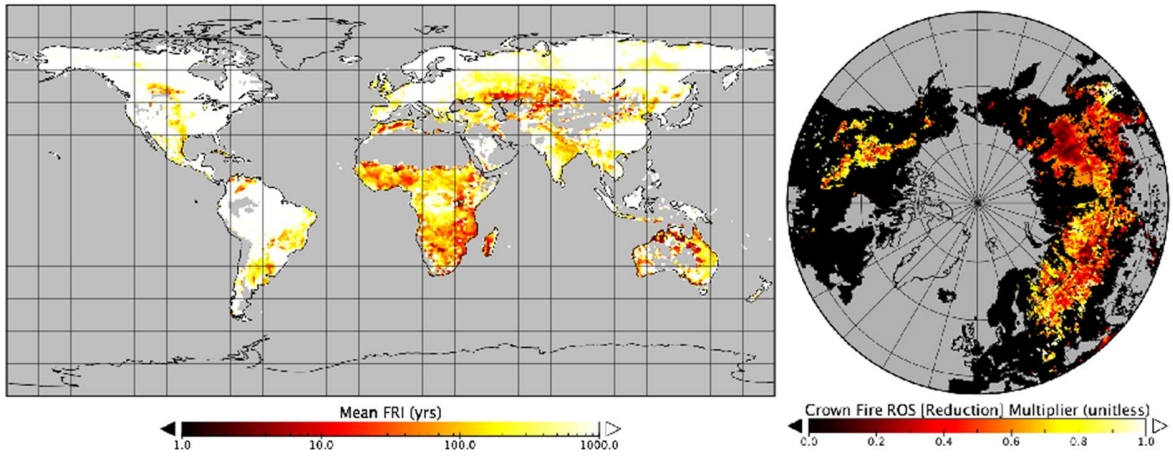


*Figure 13:* ***(Left)*** *Global grid average fire return interval (yrs fire$^{-1}$ m$^{-2}$) weighted across vegetation coverage based on output from Bowring et al. (2022) over 1901-2010.* ***(Right)*** *The PFT-weighted FRI-based crown fire ROS reduction index used to buffer crown fires in ORCHIDEE simulations (unitless). The lower the value the greater the reduction (given values are direct multipliers).*

**Solution:** The fire frequency or instance of a given region is linked to the species that are dominant in that area, which in turn is linked to fire severity. In BONA, fire frequency is low but severity high, burning largely spruce, whereas in BOEU frequency is higher, severity lower (generally ground-fire) and dominated by larch/birch. The species dominance is both driver of and driven by fire likelihood (so, a certain equivalence), so we calculate the average PFT –specific fire return interval (FRI) probability at the square meter scale over 110yrs (that is, the probabilistic FRI for any given square meter of land covered by a specific type of vegetation calculated over the period 1901-2010) and create an index based on departures of that PFT and grid cell from the median northern hemispheric FRI value for that PFT, and use this to downscale or buffer the crown fire Rate of Spread (ROS) previously calculated. We thus create a map of crown ROS-buffering factors that are based on fire frequency and vegetation type that is both potentially time and species -dynamic:

$$OS_{Red} = \Sigma(fVeg_{PFT} * (1 - (((FRI_{Grid}^{PFT} - FRI_{Global\ Median}^{PFT}) * (-1))/FRI_{Global\ Median}^{PFT}))) \quad \textbf{(5)}$$

Where $ROS_{Red}$ is the FRI based ROS reduction factor, $fVeg_{PFT}$ is the fractional coverage of a grid cell by a given PFT, $FRI_{Grid}^{PFT}$ the FRI for that PFT in a given grid cell, $FRI_{Global\ Median}^{PFT}$ the median FRI of that PFT in the N. Hemisphere. The PFT and grid-specific FRI calculations are based on ORCHIDEE-MICT simulation output for 1901-2010 from ref.(Bowring et al., 2022), and are thus model-consistent. Essentially, this method uses the Fire Return Interval as an emergent proxy for both climatological fire danger, subsequent species range dominance, and by extension evolutionary adaptation to fire disturbance. This is then used to reduce the crown fire ROS multiplier, assuming that the FRI proxy for species level fire behaviour difference can cause a maximum of a 60% reduction in crown ROS multipliers:

$$ROS_{factor} = ((U_{model} - U_{mid})/16.1) * \alpha_{ROSfactor}) * (0.4 + (0.6 * ROS_{Red})) \quad \textbf{(6)}$$

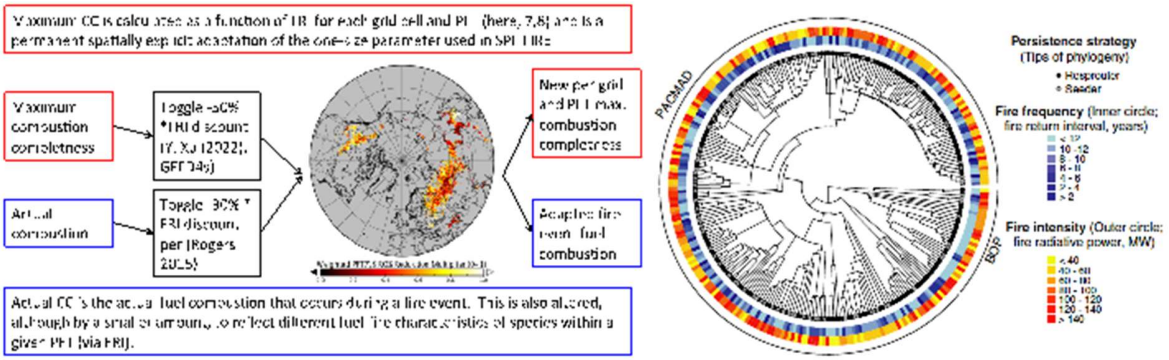


*Figure 14: **(Left)** Schematic representation of how boreal fuel combustion is modulated by ecology and proxied by the FRI index in this treatment. **(Right)** Phylogenetic chart of savannah grassland species involved in fire experiments taken from Fig. 3 of Simpson et al. (2021), showing that frequent fire species often exhibit the least intense fires.*

In ORCHIDEE-SPITFIRE, actual and maximum biomass combustion likewise cannot account for the fire regime and species-level differences that result in much more or less intense fires and ground versus crown fires. Thus, satellite-based and field observations for combustion of pre-fire biomass are also much lower in BOEU than in BONA (Xu et al., 2022, in prep.), and large amounts of standing biomass are retained on the earth surface after fire (e.g.Stenzel et al., 2019). For this reason, both the PFT aggregate maximum combustion fraction parameters in SPITFIRE as well as the actual combustion fraction simulated by it, are likely to be biased towards BONA values, given that most model parameters are derived from N. American fire research. Thus, using the $ROS_{Red}$ map produced, we reduce the PFT-specific model maximum combustion completness by -(0.5*1/ $ROS_{Red}$) and actual combustion completeness by -(0.3*1/ $ROS_{Red}$). This was performed for the three boreal PFTs initially. We are also developing something similar for tropical grassland/savannahs, based on observational confirmations of percolation theory (Cardoso et al., 2022; Laurent et al., 2019) and grassland fire ecology studies (e.g. Simpson et al., 2019 and Fig. 13).

**Problem 2: Fragmentation Representation**

**Introduction:** The impact of landscape fragmentation on fire phenomena is a complex issue primarily because its impacts are multivariate, with contradictory implications particularly for burned area. Effectively, fragmentation takes one away from 'burned area' aggregated at monthly/yearly and grid scales, and towards individual fire phenomena, resulting in opposing notions of what fragmentation can mean at these two scales. If we assume most fire-relevant fragmentation to be human-caused and not natural topographic, geomorphic, ecological fragmentation, then we take it to be a further reasonable assumption to consider roads -dirt, local, district, national and international combined - as representative of that human-scale fragmentation, given that human displacement of natural surroundings (fragmentation), in the form of various investments and infrastructure, usually requires overland access (and hence roads) for transport and travel. Based on this characterization, the following can be asserted. As fragmentation increases, (1) Annual aggregate burned area decreases (e.g. (Haas et al., 2022)); (2) Human ignition probability increases (see Koczsor, 2022, FirEURisk internal comm and deliverable); (3) Individual fire size decreases due to landscape and fuel non-connectivity; (4) Fuel moisture at the fragment edge decreases, increasing fire danger; (5) Wind infiltration and hence speed at the fragment edge increases due to decreased surface roughness, potentially increasing ROS where fires meet fragment edges. Thus, individual fires are both more probable, potentially faster spreading, yet more limited in size. These disparate effects are treated cumulatively in this version of ORCHIDEE-SPITFIRE through the Methods described below.

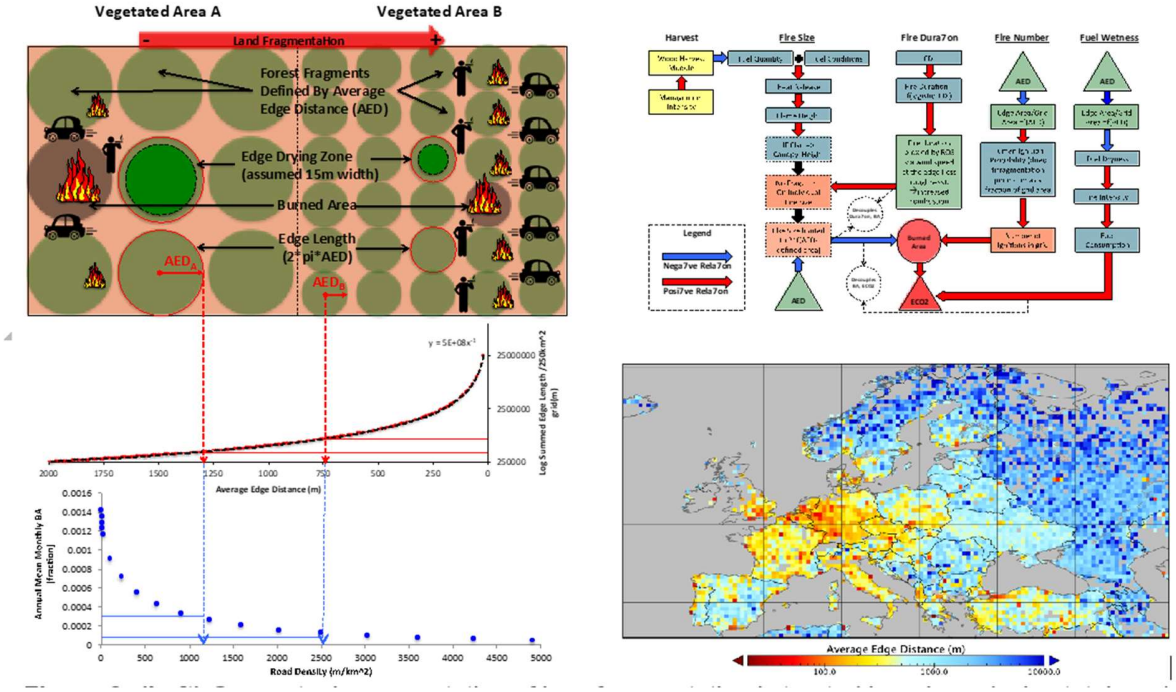


*Figure 15:* ***(Left)*** *Conceptual representation of how fragmentation is treated here by reducing total road length to circles using that perimeter, highlighting decreasing patch size and potential burned area while increasing ignitions probability. (****Top Right****) Schematic description of the model changes in ORCHIDEE to represent fragmentation.* ***(Bottom Right)*** *Map of AED solved using Eq. 7 and based on the GRIP database (Meijer et al., 2018), and used as model input for fragmentation calculations.*

**Solution:** Our fragmentation proxy here is road density, which is typically reported in metres per square kilometer, as given in Meijer et al. (2018). In order to facilitate its functional consideration within ORCHIDEE-SPITFIRE, we make the strong simplifying assumption that in any given grid cell, landscape fragments take on circular shapes of equal area. This allows for reducing road density to the average Euclidian distance to a fragment edge. This can be done by first finding the total length of road in a given grid cell by multiplying road density by grid cell area. Then, in order to reduce total grid cell road length to circular patch fragments of equal area that would satisfy that road length, and thus provide a radius or 'average edge distance' (AED) for that average patch. Thus, AED given road length sum and assuming a 0.5 degree grid cell was solved analytically and is given by the following:

$$AED = (5E08) * (1/Total\ Road\ Length) \qquad \textbf{(7)}$$

Converting road length into equal-area circle perimeters and establishing their radii strongly simplifies converting observational data to model-relevant code for representing fragmentation: **Fire size:** In ORCHIDEE, total burned area per timestep is given by the product of average fire size in a given grid cell and fire number. Thus, fragmentation should increase fire number and decrease its size. This is done first by assuming that the maximum fire patch size is three times fragment area, with the multiple assumed given to account for different patch shapes (and hence the meaning of AED). This patch size cannot be exceeded unless separate conditions are met for forests and grasslands: (1) For

forests, if the simulated fire intensity and flame height exceed canopy base height, then no size limitation is imposed. This is expected to account for the ability of high-intensity fires to 'jump' across roads. Thus, the threshold condition for crown fires used in the solution to Problem 1a is applied here in cases where the fragmentation-individual fire size limit does not hold. (2) For grasslands, Cardoso et al. (2022) found that a critical threshold in grassland fire spread related to fuel connectivity as given by area-specific fuel mass (tons/ha). If this 2.4 tons/ha grass wet mass threshold is reached, even fuel at 100% moisture was able to burn. Thus, the individual fire size limitation for ORCHIDEE grasslands is fixed only to where grass fuel mass is below this biomass threshold. **Human ignitions** (+fire number): Fragmentation increases human contact with natural patches, potentially resulting in fires through arson, cigarettes, machinery, etc. Here we assume that the increase in fragmentation causes an increase in the probability of ignitions directly proportional to the total grid cell area covered by what can be considered an edge, assuming conservatively that the human interaction with an edge can be characterized by a 1m edge to interior distance (i.e. a 1m increment into the radius of the assumed circle). We then adjust the human fire ignition function in SPITFIRE (Thonicke et al., 2010) in the following manner (Fig. 15):

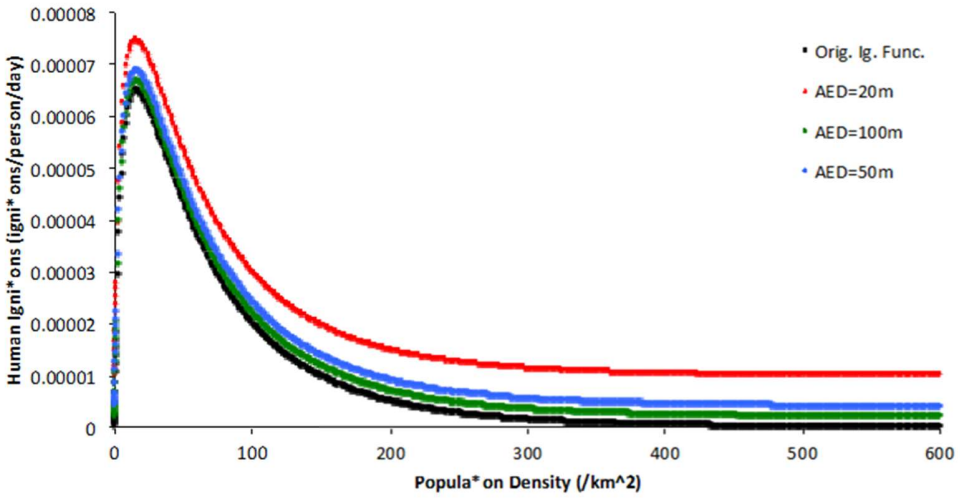


*Figure 16: How increasing fragmentation (decreasing AED) modulates the human ignition function's ignition probability for different population densities and different levels of fragmentation (different colored lines).*

$$IG_{HFrag} = IG_H + ((((2.5E08/(\pi * AED^2)) * (2\pi * AED))/2.5E08/10000) \quad \textbf{(8)}$$

Thus, an AED of 20m yields a grid area coverage of 10% of a 0.5 degree resolution grid cell. This probability is scaled to the ignitions/person/km$^2$/day as a constant (/10000). It results in significantly increased ignitions at low and high population density when fragmentation is at a maximum (AED 20m or less), which decreases exponentially as fragmentation decreases (AED increases). This is clearest at high population densities, where the suppression effect of high population is counteracted by fragmentation. **Fuel Wetness**: Landscape fragmentation studies across a large number of forested biomes have found that soil temperature and moisture was significantly higher and lower, respectively, at forest patch edge than in the patch interior (e.g. (Crockatt and Bebber, 2015; Garvey et al., 2022; Meeussen et al., 2020, 2021; Morreale et al., 2021), with subsequent impacts on fuel moisture and fire ignition and

 

spread probabilities. By conceptualizing patches as circle and assuming a linear moisture gradient from patch edge to interior, one can simply use the relative areas of patch area and edge area to define the proportion of a grid cell made subject to edge drying. Thus, we calculate the ratio of the edge area to patch area, assuming spherical patch shape, and assuming conservatively that the 'edge' through which temperature and soil effects is significant is defined as the 15m from the edge inwards (this is the distance to which edge-interior soil moisture and temperature gradient from a number of field studies falls to approximately zero). This is then the area subject to increased drying and higher temperatures owing to fragmentation:

$$AED\_Edge\_Area\_Factor = ((\pi * AED^2) - (\pi * (AED - 15)^2))/\pi * AED^2 \quad \textbf{(9)}$$

The fuel class -specific moisture thresholds ($Thresh_{FC_{1,2}}$) above which fuel consumption no longer occurs is lowered by the product of the fractional edge-to interior moisture gradient and $AED\_Edge\_Area\_Factor$, as is the actual fuel wetness:

$$Wet_{FC} = Wet_{FC} - ((0.25/2) * Wet_{FC} * \ AED\_Edge\_Area\_Factor) \quad \textbf{(10)}$$

$$Thresh_{FC_{1,2}} = Thresh_{FC_{1,2}} - ((0.25/2) * Thresh_{FC_{1,2}} * \ AED\_Edge\_Area\_Factor) \quad \textbf{(11)}$$

0.25 is the approximate fractional soil moisture gradient difference between edge and interior (0-15m) found across a range of field studies. Since we take the edge to be 15m, and assume a linear moisture gradient from 0-15m, half of the maximum gradient is taken as the average decrease in soil moisture owing to fragmentation over the length of the edge, and total grid fuel wetness is then affected by the fractional area occupied by this edge. This means that fuel moisture can at a maximum decrease by 12.5% as a result of fragmentation, amplified here by the proportional decrease in the thresholds in fuel consumption. Essentially, the edge to interior temperature is a logarithmic gradient of around 1 degree. The increase in edge area (left) with fragmentation thus raises the ambient average temperature by an exponent of AED. **Wind Speed and ROS:** Increasing fragmentation results in an increasing proportion of the landscape subject to a perimeter through which wind can travel with relatively less interruption. In other words, there is less of a barrier to wind at the edge and local surface roughness is lower, wind speeds are higher and a larger proportion of the landscape is subject to these higher winds as fragmentation increases (e.g. (De Frenne et al., 2021). We treat this in ORCHIDEE by reducing the wind speed reduction factors at lower atmospheric versus ground level by an analytically-resolved factor derived from the implicit amount of fragment edge derived from AED. Specifically, we reduce the reduction in windspeed due to tree and grass coverage in ORCHIDEE by the fragmentation area assumed by a 2m mean fragmentation depth by the fraction of total area over the grid taken up by such a fragmented area. This is done by reducing the forest and grass wind reduction factor in SPITFIRE (0.4 and 0.6, respectively) proportional to the areal coverage of the fragment perimeter assuming a 2m edge depth.

$$(f(A\_edge)_{Patch})/AED \ = \ 3.913(AED)^{-0.997} \quad \textbf{(12)}$$

Increase in windspeed in turn affects the ROS in areas that are considered substantially fragmented, leading in principle to increased BA within the patch area and (with the increase in fuel combustibility as a function of dryness and FDI), potentially greater *area-specific* total combustion and C emissions.

### 4.1.3 Results

The above developments were run for the temperate and boreal northern hemisphere (15N-90N) at 0.5 degrees resolution from 1975-2010 using imposed vegetation from ESA-LUH2, and CRU-NCEPv8 climatology. A large spatial area was chosen because potential bugs in code model code and its output sometimes only become apparent at high spatial and temporal scales in interaction with the full range of model dynamics. The code was tested in four versions: using

 

crown, crown+ROS-FRI buffer, crown+ROS-FRI buffer+fuel consumption buffer, and the three combined+fragmentation developments, and compared to a null version in which these developments had not been added (ORCHIDEE-MICT revision 5308). These are discussed below. When the crown fire code was run in isolation, burned area increased by ~10% and fire CO2 emissions by ~35% over the entire study area. Crown fires are identified directly in as an output variable in ORCHIDEE SPITFIRE as whatever fraction of a grid cell that burns under the crown fire ROS calculated. Although the increases in burned area were generally concentrated in areas where we might expect to see crown extreme fires (boreal N. America, S. Siberia, the Pacific Northwest, coastal California, northeast Mexico going into Texas, the Iberian Peninsula and Balkan region), this increase is unrealistic as crown fires are highly unlikely to occupy such a large proportion of burned area causality, and such large fractional increases in fire-relevant carbon dynamics would likely result in strong overestimates of global burned area and fire C emissions. Likewise, excess fire was simulated in North Central and East Siberia (Fig. 16a), areas that are typically associated with low intensity ground fires. When the simulation was run with the FRI ROS-modifying buffer, both crown fire-induced burned area increases and fire $CO_2$ emissions were strongly reduced (+ ~2% and ~10%, respectively; Fig. 17c) and their spatial extent more accurately corresponding to areas where crown fires are known to occur based on MODIS fire radiative power data (Fig. 16b, 16c).

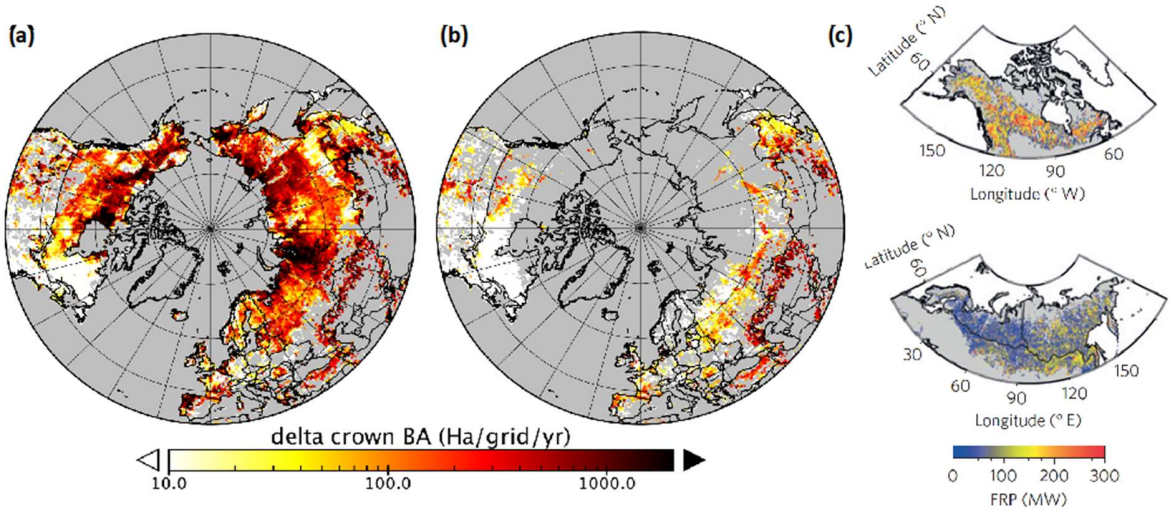


*Figure 17: Additional Burned Area from crown fire code in outputs from ORCHIDEE (a-b) and Fire Radiative Power estimates from Rogers et al. (2015).* ***(a)*** *ORCHIDEE simulation output of average annual changes in burned area over 1980-2010 (crown fire version - no crown fire version, Ha yr$^{-1}$) using only the crown fire addition in Eq. 3-4.* ***(b)*** *ORCHIDEE simulation output of average annual changes in burned area over 1980-2010 (crown fire version - no crown fire version) with the additional FRI-based sub-module to represent ecological adaptation to fires via FRI as shown in Eqs. 5-6.* ***(c)*** *Fire radiative power (FRP, MW) satellite returns averaged over 2003-2013, based on MODIS data from Rogers et al. (2015).*

To test whether there was equivalence in the observed differences in fire intensity between BONA and BOEU (average +35% FRP in BONA according to Rogers et al. (2015)), and since we cannot accurately calculate a comparable FRP metric in the model to that inferred from MODIS data, we compare this to the emissions intensity of crown fire burned area

fractions. That is, for all burned area (since the MODIS returns do not themselves distinguish between actual and potential crown fires) over the boreal region defined for simplicity as north of 50N, we the annual mass of $CO_2$ emissions per unit area of burned area for each grid cell was calculated, summed and averaged to obtain the average annual emissions intensity of fires in BONA and BOEU separately. Fig. 17a shows that rather than simulating the +35% BONA versus BOEU fire intensity difference as in Rogers et al. (2015), this model version implies the opposite dynamic, with more emissions-intense burning occurring in BOEU. However, when the emissions intensity of the model version with crown+ROS-FRI buffer+fuel consumption buffer was calculated (Fig. 17b), we find that it corresponds in principle with the Rogers et al. result, with roughly +10% more emissions-intense fires in BONA from 1980-1993, which increases to an average of +14% by 1994-2010, suggesting a gradual divergence towards more extreme fires in BONA as the Arctic climate warms, consistent with observations over the last two decades.

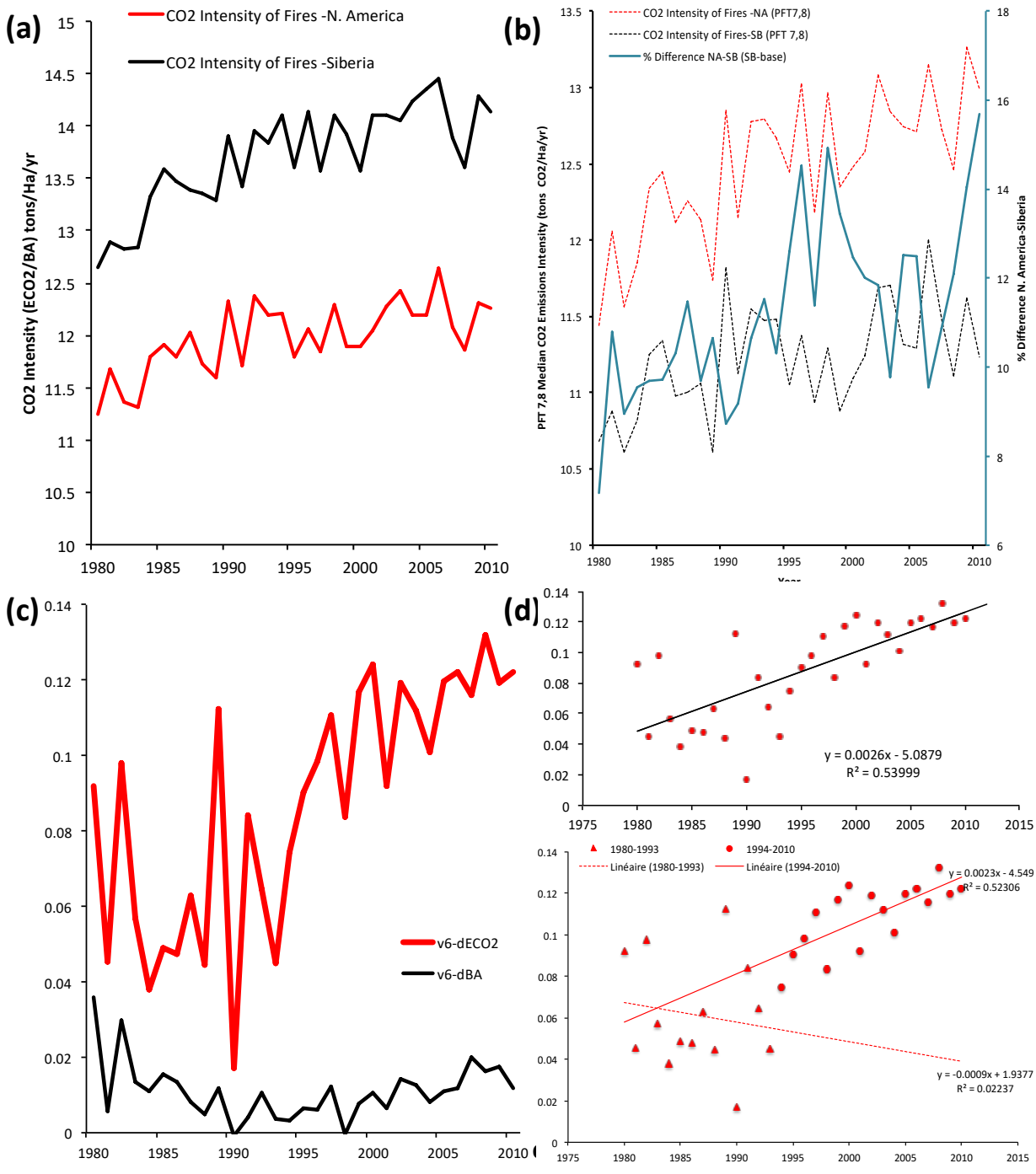


*Figure 18: Emissions Intensity Relations and Trends.* ***(a)*** *The relative $CO_2$ intensity of fire emissions (tons $Ha^{-1}$ $yr^{-1}$) over North America (red) and Siberia (black) prior to the FRI-based combustion completeness code adaptations (original fuel consumption formulation in ORCHIDEE). The relative position of the curves is inverse to that found by Rogers et al. (2015).* ***(b)*** *The relative $CO_2$ intensity of fire emissions (tons $Ha^{-1}$ $yr^{-1}$) over North America (red) and Siberia (black)*

*after FRI-based combustion completeness code adaptations, as well as the fractional difference between then (BONA-BOEU) in blue on the right-hand axis. Note the total inversion of the black and red curves relative to (a).* ***(c)*** *Relative fractional change in burned area (black) and $CO_2$ emissions (red) over the temperate and boreal N. Hemisphere over time (unitless fraction) after applying the crown fire and FRI-based code. BA remains roughly flat, whereas emissions experience a marked increase from the mid-1990s.* ***(d)*** *Top: Linear regression applied to the CO2 emissions curve in (c). Bottom: Linear regressions when applied to two time periods separately: 1980-1992 (dashed line); 1993-2010 (solid line), with regression statistics printed to show a significant trend only appearing in the second period.*

Across the whole simulation region, we found that whereas inclusion of crown fires increased total burned area by only ~2% and displayed no trend over 1980-2010, including crown fire dynamics increased $CO_2$ emissions by ~6-12%, with its trend increasing over that range over the simulation period. This is interesting because it suggests a dynamic that was recently described from observations in Zheng et al. (2021), who found that despite generally declining global burned area figures, $CO_2$ emissions from fires were increasing globally over time as climate induced extreme weather was leading to changing fuel characteristics and fire environments, ultimately causing more extreme and high-combustion fires despite burning less land area. Indeed, in Fig. 17d, we show that that whereas over the period 1980-1993 no significant temporal trend in fire $CO_2$ emissions can be found over the study period ($R^2$=0.02), a clear rising trend in crown fire-attributable $CO_2$ emissions is simulated from 1994-2010 ($R^2$=0.54). We are thus able to constrain crown fires largely to where there are known to be severe fires, and are able to show that while the addition of crown fires is a very small fraction of BA, which isn't increasing over time, the severity of crown fires (ECO2) has increased severely, as recently shown observationally. Further, adaptations to fuel consumption code result in the observed tangible difference in forest fire severity between boreal North America and boreal Siberia.

Fragmentation Output: The fragmentation-relevant code was run in additive factorial sequence, affecting (i) fire size, (ii) human ignitions, (iii) wind and ROS and (iv) fuel dryness and run over the +30N northern hemisphere over 2000-2010. The code was manipulated so that burnt area changes owing to fire size and human ignitions are explicitly output in the history file, as are changes in wind speed. Unlike the summary given in the methodology, the fire size was equal to the area determined by AED, and not three times that area. This was done because we do not know the relationship between fragment size and ultimate fire size or burned area, ad this multiplier (e.g. 3.0) may be discovered by toggling it to bring the simulated burned area vs road density relationship closer to that which is observed. By increasing the parameter from 1.0 we would thus dampen the effects of fragmentation if they are found to be too large relative to observations.

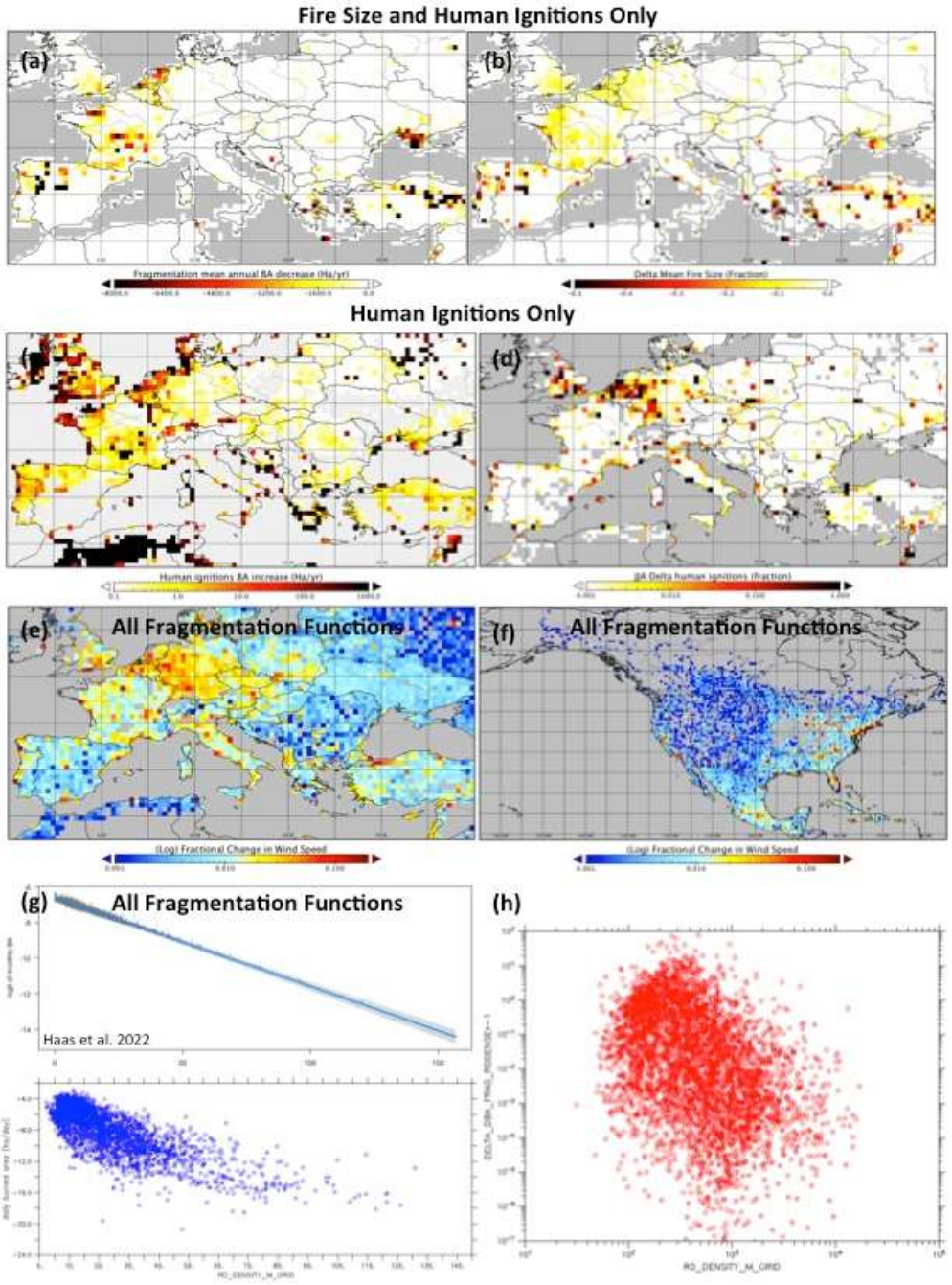


***Figure 7:***

*Figure 19:* ***Fragmentation Code Output (2000-2010 average). (a)*** *The decrease in mean annual burned area (Ha) due to fragmentation with fire size limitation and human ignitions code activated.* ***(b)*** *The fractional change in mean fire size due to fragmentation with fire size limitation and human ignitions code activated.* ***(c)*** *Increase in burned area (Ha)*

*due to human ignitions and fragmentation alone.* ***(d)*** *Fractional change in human ignitions due to fragmentation code.* ***(e)*** *Fractional increase in wind speed when fragmentation-wind speed code activated.* ***(f)*** *Same as (e) but for N. America.* ***(g)*** *Scatter plots of time-averaged monthly burned area fraction (logit-link-transformed) against the square root of road density in (top) Haas et al. (2022) from observations, and (bottom) from model output.* ***(h)*** *Log-log scatter of the change in burned area due to fragmentation and road density.*

The decrease in area burned and mean fire size due to fragmentation with (i)+(ii) combined was -0.078ha/m/km$^2$ on average over the simulated area (Fig. 18a-b), expressed in Europe by large BA decreases in central and northern Spain, the Massif Centrale in France, the Netherlands and parts of Greece. Conversely, the effect of fragmentation on human ignitions and subsequently on burned area (Fig. 18c-d) if this effect is considered alone (that is, in the counterfactual situation in which fragmentation only changes human ignitions in the model) would have led to large human ignition number increases over all regions where fragmentation is high and population density is moderate, whereas the burned area resulting from this increase in ignition number is localized in areas where population density is high or where fragmentation and population density is moderate, reflecting the shapes of the human ignition and suppression functions in ORCHIDEE-SPITFIRE. Wind speeds, which positively affect the fire rate of spread and potential area, increased due to fragmentation in the range of 0.1-30%, with changes highest in areas of high fragmentation and population density (Fig. 18 e-f). To assess the current output against observations we compared the relationship between fractional monthly burned area to road density with all fragmentation-relevant functions activated, against the same relation from observations in Haas et al. (2022).

Because of the breadth of the data's statistical distribution, Haas et al. transform these two variables, by taking the square root of road density and applying the logit-link function to burned area. The latter requires reducing a variable (burned area) to a probabilistic value, which in this case means a conversion to fraction of grid cell area ($p$). The logit function is then given by:

$$Logit(BA) = Ln\left(\frac{p}{1-p}\right) \qquad (13)$$

The comparison is shown in Fig. 18g, and shows that while the fragmentation code has yielded a comparable decreasing relationship of burned area with road density as in Haas et al. (similar slope), the intercept in our model is somewhat higher. This mismatch is encouraging, however, because the overall relationship appears to be consistent with observations (slope), and suggests that the simulated vs observed relationship could converge with 'discovery' of the mean global relationship between actual fire size and patch area -in itself a worthy scientific finding. This is work in progress, and should shortly be resolved. Finally, the log-log plot of additional burnt area declines with road density in Fig. 18h shows a generalized negative relationship, following a statistical relational form that is widely found in nature, and can be shown for a wide variety of fire-relevant variables.

### 4.1.4 Discussion

Notes on Results: The developments made to ORCHIDEE-SPITFIRE suggest that substantial improvements to representation of fire phenomena have been made. The adaptations for simulating crown fire spread are simple yet based on available observational data for temperate and boreal forests. However, this fact means that they may not be suitable for these biomes or other regions of the world for which such parameterizations have not been made. Certainly, we judged the use of a single multiplying parameter for controlling crown ROS to be unrealistic, which

is why this parameter was made a function of wind speed. The subsequent buffering of this wind modulated parameter by the FRI proxy for ecological adaptation to fire further added dynamism to the representation, and brought expected spatial extent of crown fire behavior to appear in line with what is suggested by the data from MODIS FRP returns, while the application of the same logic to fuel consumption, constrained by Rogers (2015) FRP data, allowed for the correspondence of simulation output with continental-scale observations for fire intensity, as proxied here by the emissions intensity of forest fires. While these represent substantial improvements over prior model versions, it is acknowledged that at least in principle the FRI-based approach is only a proxy that can be viewed as an emergent result of vegetation, and cannot as a result replace explicit species or clade-specific representations that would in principle yield more flexible, dynamic and finer-grained representation of different species' cause-effect relationships with fire. Nonetheless, we are confident that this is a powerful step in the right direction for efficiently representing this ecological driver, whose simplicity in function and form is well-suited to the coarse scale resolution of global land surface models. We note that it is practically difficult to directly evaluate the crown fire model outputs given that we are not aware of large-scale data that directly attributes either burned area or FRP to one or another type of fire. While we know that crown fires are rare in BOEU, that does not mean that a high intensity fire in BONA is necessarily a crown fire. Likewise, issues in satellite based FRP estimates, both in terms of their method, timing and resolution, mean that we cannot directly use the estimated area burned by crown fires to calculate the implicit FRP of those fires as compared to satellite outputs (see Bowring et al. (2022) Supplement). Finally, evaluation of the recently-developed fragmentation conceptualization and code remains at its early stages. There are a large number of assumptions made that require further research and refinement, which have not been possible at this early stage. The assumption that fragmentation is a purely human construct is obviously counterfactual. However, given that the extent of fragmentation by humans in high population density areas vastly exceeds natural fragmentation, we believe that this is a reasonable assumption for areas where road fragmentation -based AED<2000m. Nonetheless, we believe that this work already provides a powerful and efficient framework from which to begin including fragmentation as a driver of fire behavior into land surface models. In addition, the creation of a gridded time-continuous road density and AED product (see Outlook) will provide the means for researchers to adapt this framework into the future.

### 4.1.5 Outlook

Model developments for representing crown fire are now at a relatively advanced stage. The authors intend to write and publish a paper on future extreme fires in the temperate and boreal northern hemisphere to 2100, and, based on a new dataset of aboveground biomass recovery rates in these regions (Xu et al.2022, submitted), quantify the total change in standing stock carbon resulting from shifting fire regimes and species distributions. This will signal a significant advance in global-scale fire modelling, and in turn leverage the relative advantages of fire model integration into global land surface models. This exercise in turn will in itself be a useful pre-product for FirEUrisk deliverables in 2023.

Extending the FRI-based approach into grasslands will be somewhat more challenging given the species richness and ecological complexity of these biomes as compared to boreal forests, and we expect to make substantial adaptations to the approach to account for observations from fire ecologists and other relevant practitioners. Nonetheless, successful representation of subgrid-scale fire-ecological relationships would mark another profoundly useful

development in fire modelling, given that grasslands represent 70-80% of the global burned area whose modelling may require substantial conceptual improvement if model predictions for the future are to be considered reasonably robust. The agent is currently working on producing an annual time-continuous global map of gridded road density to 2100. This will be useful for predicting fire behavior in the future do to fragmentation, as well as serve the interests across domains from urban planning to conservation ecology.

The multi-faceted representation of fragmentation laid out here requires further development and testing across multiple scales. Nonetheless, the agent believes this high simplification of fragmentation provides a unified and relevant framework through which to represent the often-confounding effects of fragmentation on fire behavior, made possible by distilling patches into circles and fragmentation into an aggregated perimeter length defined by roads. By refining this representation specifically for Europe, whose landscapes are on average the world's most fragmented, we hope to cover a highly relevant and dynamic driver of fire behavior for assessing future fire risk in Europe.

The large number of model bugs discovered within the original SPITFIRE code will require resolution. There are elements of the existing model that have been chosen to be counterfactual, such as the limitation of fire duration to four hours, in order that the model does not produce vastly unrealistic burned area estimates. Fixing these bugs, which mostly suggest that the existing model contains strong overestimations of fuel consumption and ROS, might allow for realistic fire times to be simulated, and in turn hugely benefit the model by bringing the whole edifice directly within the full remit of observational fire science.

# 5 Projecting future fire danger (Ignition by lightning)

## 5.1 Introduction

A challenging task of fire forecasting has been approached in climatological mode, i.e., based entirely on meteorological scenarios (or for long meteorological archives, such as ERA-5) and without any observational information on fires. This challenge has been approached by extending the forecasting methodology developed by FMI, which relies on a thorough investigation of the statistical properties of the data at hand and possible physics-based relations between the parameters. The essence of the methodology is to establish a "static mapping", i.e., a set of non-linear statistical dependencies between a set of predictors and the predicted variable.

The Fire Forecasting Model FFM v.1.0 predicts the Fire Radiative Power (FRP), which is directly comparable with, e.g., MODIS FRP. The core of the model has been developed within the EU Horizon project EXHAUSTION and Academy of Finland HEATCOST. The new addition developed within FirEUrisk to that model is natural ignition by lightning. The prediction time horizon is unlimited since the model can operate at climate-relevant scales, both in past and future, using only meteorological predictions produced by weather forecasting and climate models.

The FFM is a part of a new release of the Integrated System for Wildland Fires IS4FIRES (http://is4fires.fmi.fi), (Soares et al., 2015; Sofiev et al., 2012, 2009), which uses the FRP retrievals of MODIS instruments onboard of Aqua and Terra satellites and produces time- and space- resolving 4-D emission flux for 21 atmospheric pollutants. The new version of IS4FIRES incorporates the fire information from VIIRS and the FFM v1.0.

## 5.2 Methods and data

**Input datasets**

- The MODIS FRP collection 6 fire detection procedure is based on an algorithm of Wooster (2003) that exploits the strong emission of mid-infrared radiation from fires. Details on the way the MODIS FRP is used by IS4FIRES are described in (Soares et al., 2015; Sofiev et al., 2009).
- The ERA5 reanalysis (European Reanalysis v.5, https://www.ecmwf.int/en/forecasts/datasets/reanalysis-datasets/era5) is a global meteorological dataset, which provides hourly estimates of atmospheric, terrestrial, and oceanic meteorological variables. The data covers the globe with a ~25km grid and resolve the atmosphere with 137 levels from the surface up to a height of ~80km.
- The CESM (Community Earth System Model, https://www.cesm.ucar.edu/experiments/) climate predictions are used for both historical era and for future SSP (Shared Socioeconomic Pathways) scenarios (Meinshausen et al., 2020). The CESM meteo exists with one hour time resolution and about 1-degree spatial resolution (288 longitude and 192 latitude points). For future scenarios, the years 2015-2100 have been provided by CICERO to FMI for the SSP126 scenario ("sustainability"), the SSP245 scenario ("middle-of-the-road"), and the SSP370 scenario ("regional rivalry").

The statistical methodology adapted to fire forecasting has its roots in the ground-setting works of Voeikov Main Geophysical Observatory for urban air pollution (Berlyand, 1991; Genikhovich et al., 2004). This approach has been adapted by the FMI team, in collaboration with University of Latvia, to a variety of tasks (Ritenberga et al., 2016, 2018; Sofiev et al., 2017). However, the statistical features of the fire problem represent an extreme case, which required more complicated arrangements. Since the prediction of individual fire ignition is meaningless, the problem uses spatial and temporal averaging with adjustable kernels to catch the mean and/or upper percentiles of the fire events. Apart from non-linear transformations described by Ritenberga et al., (2016, 2018) and Sofiev et al. (2017), the following additional transformation steps cope with peculiarities of the fire prediction problem:

- MODIS detection limit was parameterized generally following the procedure of (Maier et al., 2013), who estimated it for FRP Collection 5 data in Australia. Modification of that analysis leads to a simple analytical parameterization of MODIS detection limit applicable over the globe.
- SEVIRI-based parameterization of diurnal FRP variation of IS4FIRES v.1.0 has been reviewed by adjusting the day-night spread but keeping the profile shape intact.
- Five popular fire danger indices (FDIs) have been reviewed and their coefficients re-optimized using MODIS fire detections as a fitting target: Fire Weather Index (Van Wagner and Pickett, 1985), Keeth-Byram drought index KBDI (Keeth and Byram, 1968), soil drought index SDI as quoted by (Kumar and Dharssi, 2015), McArthur grass fire danger index as presented by (Schreck et al., 2010).
- Due to episodic character of fires, the normalization step had to be skipped in the pre-processing and replaced with the post-processing alignment of distribution functions. This was realized as a point-by-point rescaling of quantile chart towards the 1:1 relation.

**Lightning ignition outlook**

Lightning is a dominant natural cause of fires. The FFM v.1.0 has been based on grid cell-oriented approach. This allowed easy representation of sharp spatial gradients and reflect the differences in anthropogenic ignitions from one region to another. However, no proxies were added for incorporation of lightning as a precursor of fires. This shortcoming has been rectified within FirEUrisk by including the meteo-models predictions for lightning. A detailed presentation of the fire ignition module is provided in the WP1 deliverables. Its impact is quite sporadic in time and sparse in space but still accounts for a few % of adjustment in the FRP release, in a broad agreement with estimated contribution of lightning into the overall fire patterns of ~10%.

**Impact of meteorological drivers**

A potentially very significant problem was the difference between climatological models like CESM and standard weather forecasting models, such as IFS. That difference, exacerbated with the data assimilation applied in standard weather forecasting tasks, would lead to potentially crucial differences between the actual meteorological situation, as represented in the reanalysis archives and weather forecasts, and climate scenarios run retrospectively for the same period. As a result, the FFM calibrated to predict actual fires observed by MODIS using the actual-meteo reanalysis ERA5 would fail to reproduce the retrospective fire patterns when driven by the retrospective-climate scenario. This would undermine the credibility of the fire computations for the future-climate scenarios.

To verify the effect, FFM was run twice for the retrospective period – driven by ERA-5 and by CESM historical simulations.

## 5.3 Results

**Effect of different meteorological drivers on fire predictions**

The impact of the meteorological drivers was checked by comparing the predicted fires for ERA-5 and CESM-history meteorological predictions. Since the CESM run was not associated with any specific time line, only mean statistics were comparable.

As seen from the comparison of mean annual FRE (Fire Radiative Energy), the FFM predictions for ERA-5 and CESM-history appeared quite comparable. Since spatial distribution of the fire activity is, by construction, tied to the observed fires, we conclude that the switch between ERA-5 and CESM meteo fields does not lead to an excessive difference in the fire totals, and the system can be applied for the future climate scenarios.

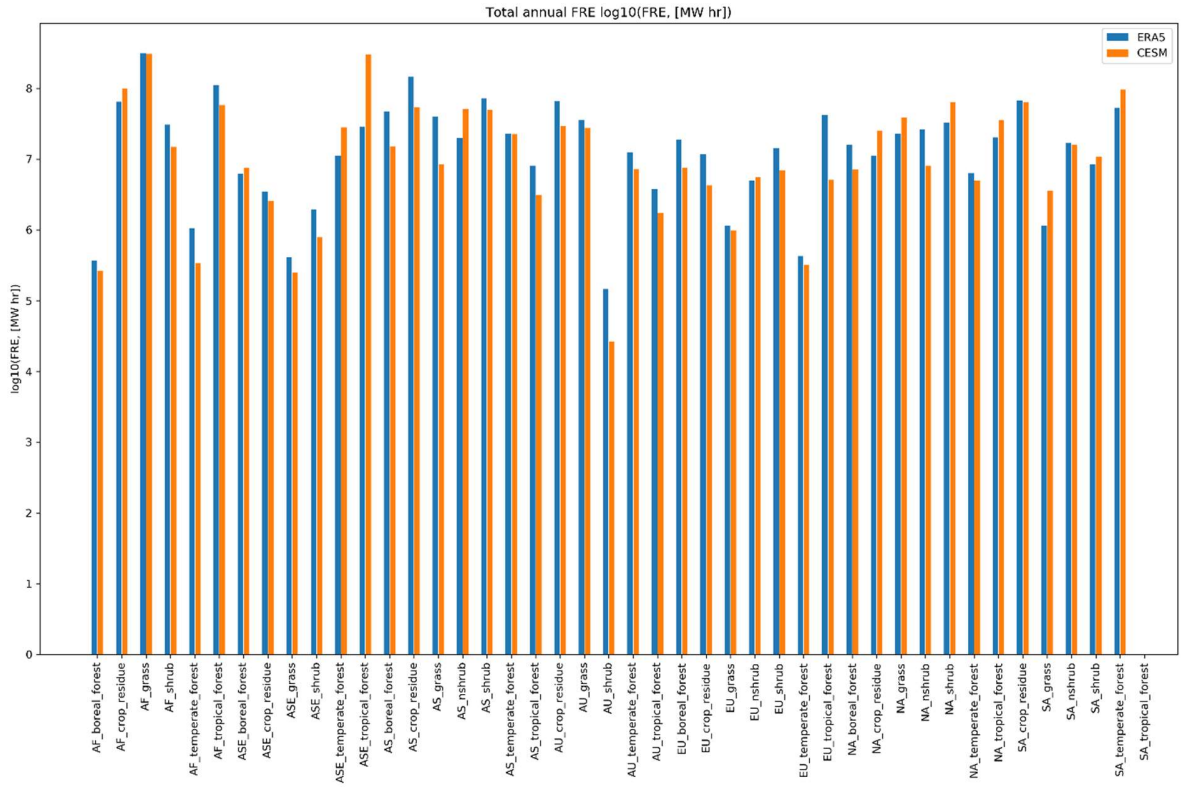


*Figure 20: Mean annual Fire Radiative Energy predicted for retrospective periods by FFM v.1.0 when driven by the ERA-5 reanalysis and by the CESM past-climate simulations.*

**Fires for the future climate scenarios**

IS4FIRES system was applied to the CESM future climate scenarios, replacing the driving meteorological stream with climatological predictions. The obtained time series represent the fire emission projections for the respective climatological scenario.


*Figure 21: Example of FRP predictions, CESM SSP245 future scenario.*

## 5.4 Outlook

The problem of projecting future fire danger was approached with the current Fire Forecasting Model version 1.0, which is the first practically applicable model capable of reproducing the main features of the fire seasons in Europe and, with some reservations, over the globe. Its time series seem to satisfy the requirements of the climatological-scale applications. The main unresolved issue refers to handling the strongly non-Gaussian distribution function of FRP. The current approach ensured formal identity of the distribution functions and allowed usage of the data in downstream applications but left the core of the problem unresolved. This topic is closely related to the MODIS detection limit, which is partly behind the unusual features.

# 6 Species distribution and phenology model Phenofit

### 6.1.1 Objectives

Tree species with their biomass, their architectural structure and their functioning as response to drought and fire, both affect and are affected by fires. Climate directly affects their water and carbon budget, particularly their canopy leaf biomass and moisture content on a daily time scale, but also growth, death and regeneration through flowering, seeding and germination processes and in turn their continental distribution on the longer term. Projecting future hazard, but also the subsequent ecosystem vulnerability through potential loss, resistance and recovery time will highly depend on their future distribution. We propose here to couple a process-based species distribution model PHENOFIT designed to capture the climate effects on the success of reproduction phases as the main constraint on species presence, and an ecohydrological model stating that forest structure (tree height and tree cover) is optimized to cope with drought by reducing tree cover (and then transpiration) while keeping optimized tree growth and carbon assimilation. We hypothesize here that species presence coupled with its vertical and horizontal fuel structure might highly drive fire hazard (Van ness et al., 2018).

### 6.1.2 Methods and data

PHENOFIT is a process-based species distribution model for forest tree species which focuses on phenology. It relies on the principle that the distribution of a tree species depends mainly on the synchronization of its timing of development to the local climatic conditions (Chuine & Beaubien, 2001). It is composed of several submodels, including phenology models for leaves, flowers and fruits, and stress resistance models. It simulates the fitness (survival and reproductive success) of an average individual using daily meteorological data, soil water holding capacity and species specific parameters (Figure 21) . PHENOFIT has been validated for several North American and European species by comparing their known distribution to the modeled fitness (e.g. Morin et al., 2007; Saltré et al., 2013; Duputié et al., 2015; Gauzere et al., 2020).

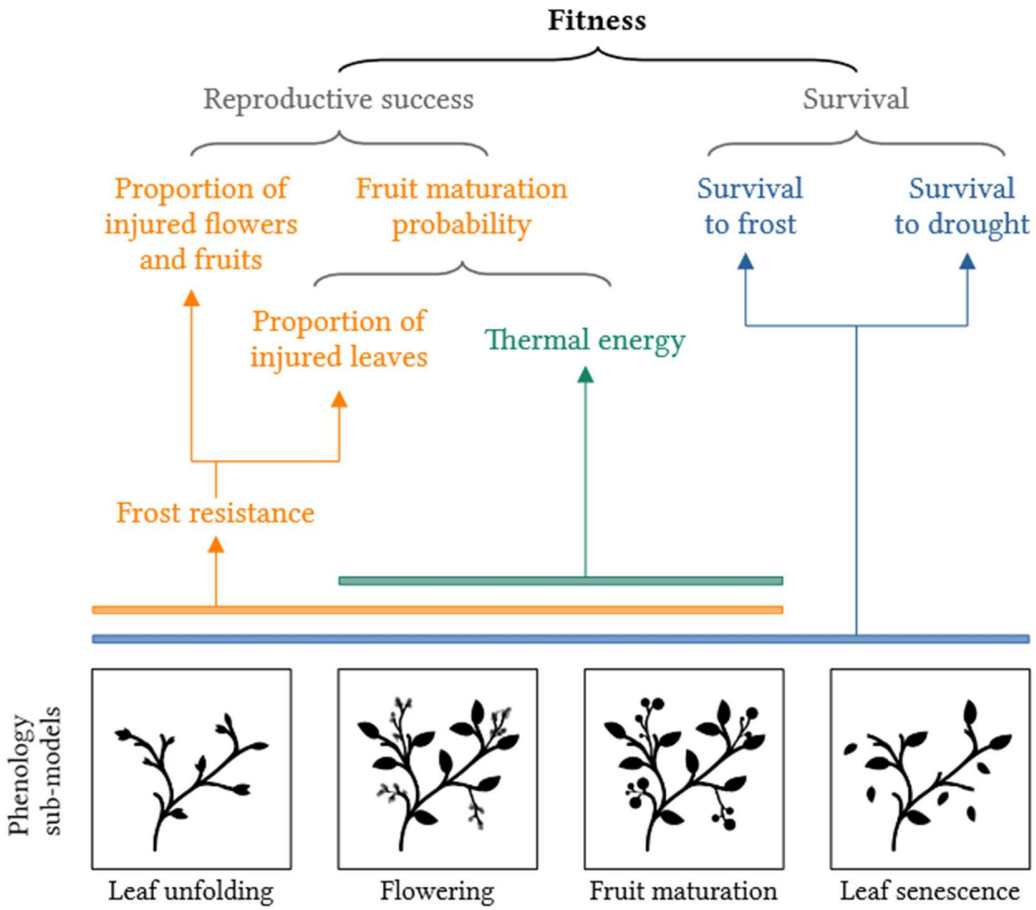


*Figure 22: PHENOFIT conceptual scheme.*

The hydroecological SIERRA model simulates a daily tree cover water and carbon budget through species traits as leaf Area, root profile, stomatal closure processes, and water use efficiency (Mouilot et al., 2001), controlled by daily climate and soil profile and texture. Daily actual evapotranspiration is calculated from the potential evapotranspiration, leaf surface, and stomatal conductance derived from the plant water potential. The daily plant predawn water potential is calculated from the daily soil water content along the root profile and its texture according to the Saxton equation. Soil water content is updated daily by precipitation inputs, and actual plant evapotranspiration proportionally distributed in the soil layers according to the root profile. From the daily plant transpiration, gross carbon assimilation GPP is calculated by the specific maximum Water Use Efficiency (WUE), controlled by the daily vapor pressure deficit derived from daily temperatures. Plant autotrophic respiration R is calculated according to leaf biomass amount and a Q10 function of air temperature, with the net primary production NPP=GPP-R. From these daily simulations of plant water potential and carbon assimilation, we could derive the drought onset, being the day of the year T0 when plant water

potential is below -1.1MPa and identified as the threshold when trunk radial/vertical growth is blocked by the lack of cell turgescence, and the yearly carbon assimilation NPP.

### 6.1.3 Data for the calibration

**Climate and soil data**

Raw climatic variables were extracted from ERA5-Land hourly dataset (Muñoz Sabater, 2019, 2021) from 1970 to 2000, at a spatial resolution of 0.1 degree in latitude and longitude. We calculated the daily mean values of the following variables used by PHENOFIT and SIERRA: minimum, mean and maximum daily temperatures, mean dew-point temperature, daily precipitation, daily global radiation and daily mean wind speed. We computed the daily relative humidity with the ratio of vapor pressure and saturation vapor pressure (both calculated with Clausius-Clapeyron equation) using humidity R package (Cai 2019). Daily potential evapotranspiration was calculated with the Penman–Monteith equation (FAO standard of hypothetical grass reference surface) using a slightly modified version of the ET() function in the Evapotranspiration R package (Guo et al. 2016). Water content at field capacity and wilting point data were extracted from EU-SoilHydroGrids (Tóth et al. 2017) which is at 1km resolution. Percentage of sand, silt and clay particles, percentage of coarse fragments, bulk density and soil depth were extracted from SoilGrids250m (Hengl et al., 2017) at a 250m resolution. These data (except for soil depth) are provided at seven soil depths, so we summarized them (weighted sum or weighted mean) taking into account each layer width and total soil depth. Finally, all variables were upscaled at the ERA5-Land spatial resolution 0.1°.

**Tree occurrences in Europe**

The occurrence data we used essentially rely on the EU-Forest dataset (Mauri et al., 2017) which benefits from inventory and monitoring programmes implemented in most European countries. As EU-Forest is limited to forest ecosystems, we completed it with presence records extracted from the Global Biodiversity Information Facility (GBIF 2022) but removing observations outside natural species ranges as defined by Atlas Flora Europeae (AFE, Jalas & Suominen, 1972–2005) and EuroVegMap (Bohn et al., 2003). By doing so, we also included occurrences of isolated native trees living outside forests, excluding records from arboreta or gardens where the species would have been planted as an exotic. For holm oak, we also added occurrence records in the Mediterranean Basin from the WOODIV database (Monnet et al., 2021), leaving out EU-Forest and GBIF records we had already gathered. We upscaled all species records at the ERA5-Land resolution (i.e. 0.1° cell, see 1.2.1. Climate data). We finally obtained 21458 occurrence cells for beech, 6653 for holm oak and 5385 for silver fir.

**Phenofit calibration**

Covariance Matrix Adaptation Evolution Strategy (CMA-ES) was used as a robust optimization algorithm for non-linear, non-convex, as well as non-separated optimization problems in continuous domain (Hansen & Ostermeier, 1996; Hansen & Ostermeier, 2001; Hansen, 2006). It is based on the principle of evolutionary biology, via recombination, mutation and selection of the most fit individuals (i.e. parameter sets providing the best predictions). One of the advantages of CMA-ES is that it does not require a complex parameter tuning: as best parameter values at a given time of the optimization process might no longer be efficient later, CMA-ES implements an internal adaptation of its parameters. We only chose the population size λ, depending on the optimization problem complexity (μ was set to

λ/2). The default recommended value for λ is 4 + 3ln(N ), where N is the number of parameters to calibrate (i.e. λ ∈ [14, 17] in our case). We set λ = 20, in order to improve the global search capability (Hansen & Kern, 2004) and take advantage of the computation power at our disposal. All model parameters were linearly scaled into [0; 10] so that the same standard deviation can be applied to all parameters: here we chose σ = 2 (for practical hints on variable encoding, see Nikolaus Hansen personal website : http://www.cmap.polytechnique.fr/~nikolaus.hansen/). Our stopping criterion for the optimization procedure was the budget, i.e. the number of model runs. We used a pure R implementation of CMA-ES available in the R package cmaes (Trautmann et al., 2011). The function cma_es() enables us to do λ function evaluations in parallel so as to substantially reduce computation time. It also allows us to define lower and upper bound constraints, by penalizing individual fitness (i.e. objective function value) if it violates the boundaries. We customized the cma_es() function to add an option to define death penalty constraints (rejection of the infeasible individual who is sampled again), in order to define a range of ecologically possible solutions in terms of inequality constraints between parameters.

An objective function for the calibration was the area under the receiver operating characteristic curve (AUC), evaluated against a subset of 2000 points. We used the AUC R package (Ballings & Van den Poel, 2013), and chose the two following model output variables as proxies of classification probabilities (i.e. used to determine if the species can be present or not): fitness index for PHENOFIT. Regarding the PHENOFIT model, we calibrated ten times each species parameter set using CMA-ES algorithm, with 5 repetitions on 2 random subsets of presences/pseudo-absences (see 1.2.2. Tree occurrences), except for beech. In the latter case, we ran 10 repetitions on 10 subsets (i.e. 100 calibrations) to investigate both the effect of subsampling and the effect of stochasticity on the calibration performance of CMA-ES.

**Optimal tree height/tree cover (TH/TC)**

To test and design our optimal TH/TC from the SIERRA hydroecological model, we ran the SIERRA model on the 30-year climate time series over a random sample of 100 sites in Europe to get the T0 and GPP values. For each sampled site, we performed 10 simulation runs with Tree cover (TC) varying from 10% to 100% with a 10% step. For each TC value on a given site, we get T0 and NPP. From these 10 triplet values (TC, T0, NPP), we kept the TC and T0 values for which NPP is the highest, as the optimal TC generating the maximum carbon assimilation and generating a given T0. By decreasing tree cover (and Leaf Area index), transpiration is more limited, so that we systematically get a delayed T0 when reducing tree cover (Cabon et al., 2018). On the other side, ecosystem NPP tends to decrease with decreasing tree cover, but under water limited ecosystems with a prolonged dry period when carbon assimilation is low, the maximum NPP is not systematically obtained at 100%. Dense tree cover generates a leaf mass respiration hard to sustain with the given assimilation. For each sample site, we then obtained values of TC and T0 for which NPP is the highest. T0 has been shown to be highly correlated to interannual radial tree growth on a yearly basis for a given forest stand (Lempereur et al., 2017), so that the more delayed is the drought onset, the larger is the tree. Tree architecture also shows a strong relationship with tree diameter at breast height (DBH) and tree height. We then converted T0 into a tree height value. However, the root/shoot ratio is hardly conserved across drought gradients (Cabon et al., 2018b), so that tree architecture can vary according to drought, with increasing root proportion when the climate is drier. We then calibrated a nonlinear function converting T0 into tree height TH as a response to T0 based on the global three height and tree cover maps (Hansen et al., 2013, Potapov et al., 2020).

### 6.1.4 Results

Calibrations using species distribution data, CMA-ES, are thereafter called backward calibrations, and calibrations based on expert knowledge, observations and measurements of the processes modelled are called forward calibrations. CMA-ES calibration of PHENOFIT model allows an average 17.2% increase of AUC across the three species compared to forward calibration (Figure 23). The maximum increase is obtained for silver fir, from 0.72 to 0.9 (25%). This first phase of the model calibration for three main dominant species in Europe can be used for climate model projections.

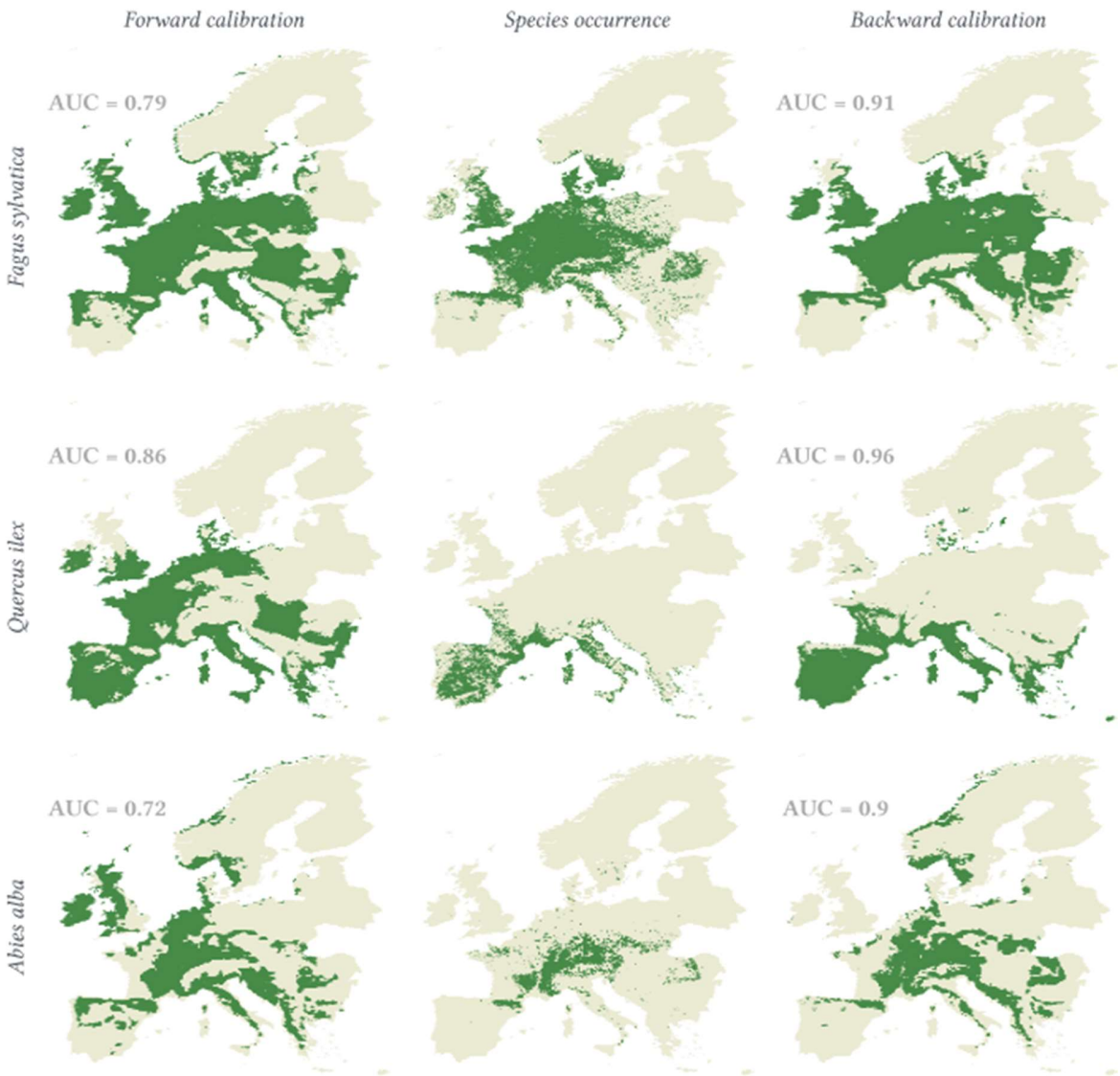


*Figure 23: Species distribution maps obtained with PHENOFIT forward and backward calibrations, compared with observed species occurrences. Optimal threshold to dichotomize the model predicted fitness index in presence/absence is the Youden index-based cut-off point.*

Regarding the TH/TC model, Figure 24 illustrates our early results on the TC/TH relationships simulated for 100 sample sites with contrasted climates across ET. Our approach could simulate a self-organized varying optimal TC according to drought conditions, and generating decreasing tree height, a spatial pattern actually observed on the driest range of the mediterranean climate. The model is ready for ET applications and validation with observed TH/TC from remote sensing across ET.

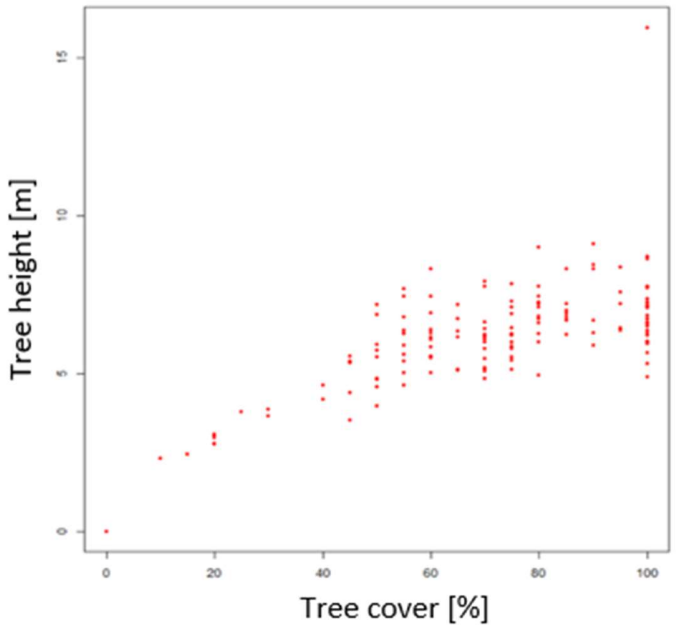


*Figure 24: Optimal tree height (m) and tree cover (%) obtained from the optimal tree growth/Carbone assimilation model across 100 sample sites in the European territory climate gradient. Target species is* holly oak *(Quercus ilex).*

### 6.1.5 Outlook

The coupling of PHENOFIT with a forest structure model allows for a climate-driven distribution of forest species across ET, with a structural representation of the canopy as tree height and tree cover. Combining this information feeds the varying fuel map for future fire hazard projections as well as its moisture status assuming that canopy water status varies across species functioning. The information on tree height and tree cover delivers the vegetation structure hardly assessed with other projections mostly focused on presence and biomass, while canopy density and vertical continuity of fuel influences fire spread and litter to canopy flaming transfer. Species future distribution and TH/TC also deliver the information for ecosystem potential loss (in terms of biomass, carbon and wood or ecosystem value), and recovery depending on their regeneration and fire resistance/resilience traits, as part of the Ecological vulnerability assessment task. Only a few dominant tree species can be simulated with this approach, limiting applications on plant biodiversity

assessment. However, forest structure is a significant component for habitat characterization and bird/mammal diversity.

# 7 Synthesis

Overall, the goal of our work was to improve the accuracy and reliability of fire-enabled DGVMs in order to better understand and predict the interactions between vegetation and fire, particularly in areas with strong human influences such as Europe. This is achieved through the incorporation of machine learning approaches, the improvement of predictions for human-caused ignitions and lightning-caused ignitions, and the better representation of extreme fires. Additionally, we aim to improve the quality of vegetation predictions through the use of the species distribution model PHENOFIT. By improving these elements, we hope to better understand and predict the impacts of fire on vegetation in European landscapes.

## 7.1 Use of simulated fuel load in fire effect models

Fire-enabled DGVMs simulate changes in vegetation composition and related fuel production under changing climate. Land-use and demographic changes fragment the landscape, thus fuel bed and the way humans use the landscape which causes fire - accidentally and intentionally; in the latter case to manage the landscape. Fire-enabled DGVMs can compute related changes in human-caused ignitions depending on human population density and the distance to road density and their effects on burned area and fire effects. Therefore, they will project changes in propagation, ignition, exposure and vulnerability to support the quantification and assessment of future risk conditions where the consequences of the projected changes in vegetation, dead fuel and fire regimes on environmental services, ecological values and resilience will be assessed.

The simulation results from the fire-enabled DGVMs, even though conducted at 9 km grid cell resolution, are still too coarse for in-depth analysis at the landscape scale because within a 9 km grid cell the models subdivide natural and managed land depending on the prescribed land-use input, these proportions are not spatially explicit which is an important factor with respect to landscape fragmentation. Given the modelling objective to represent fire and vegetation dynamics at the coarse and global scale, these models do not resolve the dynamic of individual fire events or how fuel arrangements may affect fire propagation at the landscape scale. In addition, fire effects on species composition, where fire-enabled DGVMs aggregate vegetation composition into Plant Functional Types (PFT) to be representative at the biome level, can be resolved better when connecting process-based detail at the landscape scale using information from species distribution models. Here, detailed process-based models, species-based models and fire propagation and fire effects models at the landscape scale which do not resolve the long-term changes in vegetation, hence fuel composition and fuel load, can make use of the projected long-term changes in vegetation and fuel under climate and land-use change for the 21st century.

Fire-enabled DGVMs will provide output variables that could estimate fuel properties, i.e. fuel load per dead fuel class, PFT composition, dead and live biomass, and fire ignitions, burned area and dead and live fuel consumed by fire within a 9 km grid cell covering the ET scale from 2015-2100. Additional effort should be required to convert PFT into fuel

categories, as much similar as possible to those defined by the FirEUrisk classification system, so some of the parameters included into standard fuel models could be estimated for future conditions.
Time slices of the detailed variables will be provided so that high-resolution models operating at the PS and/or DA scale can make use of these coarse representations of fire ignition, fuel characteristics for modeling future propagation and effects characteristics, in order to better capture detailed changes in the local context of DA and PS. Meta-data information and map projections will follow the guidelines of the data platform so that the results are interchangeable among users.

## 7.2 Outlook on future projections of fire at European Scale

In terms of simulating of future projections (2015-2100) we identify three drivers that could change significantly from the historical period (1950-2014): climate, socio-economic conditions and land-use. Climate induced fire risk has been studied and applied for many years (e.g. Canadian Fire Weather Index). Warmer and drier conditions in the future are expected to increase the frequency and intensity of fires, which could have significant consequences for vegetation and ecosystems, especially in Mediterranean areas. The models used here, reflect the changing climate by including transient climate projections from historical climate (ERA 5) to future climate realizations of the shared socioeconomic pathways (ssps126, ssp245, ssp370 and ssp585). Additionally, they provide deeper insights on climate effects on the vegetation and fuel dynamics. However, there are still some challenges in representing the effect of extreme weather conditions that might not lead to suitable responses of the simulated vegetation. The implementation of e.g., crown fires and multiday burning presented in this report is a first step in the direction of representing extreme fires of the future.
The influence of socio-economic drivers is currently still challenging, as they can have amplifying effects (through increasing ignition) and suppressing effects (e.g., by landscape fragmentation) that are difficult to disentangle. With the improvements presented in this Deliverable, we incorporate the most recent findings of human-driven processes in DGVMs. Further possible human interactions (advanced fuel management) are already being tested, but should be further investigated to provide valuable information for fire management and planning efforts.
To use the full potential of the coupled vegetation-fire modelling approach, another important next step will be to use the DGVMs with a more regional vegetation representation of Europe and land-use. Based on high-resolution land-use scenarios associated to the shared socioeconomic pathways currently developed in Task 3.1 and new insights from species distribution models, we see the potential to represent fuel composition and dynamics more accurately for present and future simulations.

# 8 References


Albini, F. A.: Estimating wildfire behavior and effects, Dep. Agric. For. Serv. Intermt. For. Range Exp. Stn., 30, 1–22, 1976.

Ballings, M. & Van den Poel, D. (2013). AUC: Threshold independent performance measures for probabilistic classifiers, [R-package] https://rdrr.io/cran/AUC/man/AUC-package.html

Batjes, N.H., Leenaars, J.G.B., Ribeiro, E., Wheeler, I., Mantel, S. & Kempen, B. (2017). SoilGrids250m: Global gridded soil information based on machine learning. PLOS ONE, 12, e0169748

Berlyand, M.E., 1991. Prediction and Regulation of Air Pollution. *Springer Netherlands*. https://doi.org/10.1007/978-94-011-3768-3

Bohn, U., Neuhäusl, R., Gisela Gollub, Hettwer, C., Neuhäuslová, Z., Raus, T., Schlüter, H. & Weber, H. (2003). Map of the natural vegetation of Europe - scale 1:2500000, *Landwirtschaftsverlag, Münster*

Bowring, S. P. K., Jones, M. W., Ciais, P., Guenet, B. and Abiven, S. (2022): Pyrogenic carbon decomposition critical to resolving fire's role in the Earth system, Nat. Geosci., 15(2), 135–142, doi:10.1038/s41561-021-00892-0

Breiman, L. (2001). Random Forests. *Machine Learning*, *45*, 5-32. https://doi.org/10.1023/A:1010933404324

Byram, G. M.: Combustion of forest fuels., in Forest fire: control and use, pp. 61–89., 1959.

Cabon A., Mouillot Florent, Lempereur M., Ourcival J. M., Simioni G., Limousin J. M. (2018). Thinning increases tree growth by delaying drought-induced growth cessation in a Mediterranean evergreen oak coppice. *Forest Ecology and Management*, 409, p. 333-342. ISSN 0378-1127

Cabon, A, Martínez-Vilalta, J, Martínez de Aragón, J, Poyatos, R, De Cáceres, M. (2018). Applying the eco-hydrological equilibrium hypothesis to model root distribution in water-limited forests. *Ecohydrology*., 11:e2015. https://doi.org/10.1002/eco.2015

Cai, J. (2019). Humidity: Calculate water vapor measures from temperature and dew point

Cardoso, A. W., Archibald, S., Bond, W. J., Coetsee, C., Forrest, M., Govendere, N., Lehmann, D., Makaga, L., Mpanza, N., Ndong, J. E., Pambo, A. F. K., Strydom, T., Tilman, D., Wragg, P. D. and Staver, A. C. (2022): Quantifying the environmental limits to fire spread in grassy ecosystems, Proc. Natl. Acad. Sci. U. S. A., 119(26), 1–7, doi:10.1073/pnas.2110364119,

Chuine, I. & Beaubien, E.G. (2001). Phenology is a major determinant of tree species range. Ecology Letters, 4, 500–510.

Crockatt, M. E. and Bebber, D. P. (2015): Edge effects on moisture reduce wood decomposition rate in a temperate forest, Glob. Chang. Biol., 21(2), 698–707, doi:10.1111/gcb.12676

Cruz, M. G., Alexander, M. E. and Wakimoto, R. H. (2005): Development and testing of models for predicting crown fire rate of spread in conifer forest stands, Can. J. For. Res., 35(7), 1626–1639, doi:10.1139/x05-085

Cucchi, M., P. Weedon, G., Amici, A., Bellouin, N., Lange, S., Müller Schmied, H., Hersbach, H., & Buontempo, C. (2020). WFDE5: Bias-adjusted ERA5 reanalysis data for impact studies. *Earth System Science Data*, *12*(3), 2097–2120. https://doi.org/10.5194/ESSD-12-2097-2020


 

De Frenne, P., Lenoir, J., Luoto, M., Scheffers, B. R., Zellweger, F., Aalto, J., Ashcroft, M. B., Christiansen, D. M., Decocq, G., De Pauw, K., Govaert, S., Greiser, C., Gril, E., Hampe, A., Jucker, T., Klinges, D. H., Koelemeijer, I. A., Lembrechts, J. J., Marrec, R., Meeussen, C., Ogée, J., Tyystjärvi, V., Vangansbeke, P. and Hylander, K. (2021): Forest microclimates and climate change: Importance, drivers and future research agenda, Glob. Chang. Biol., 27(11), 2279–2297, doi:10.1111/gcb.15569

Drüke, M., Forkel, M., Bloh, W. Von, Sakschewski, B., Cardoso, M., Bustamante, M., Kurths, J., & Thonicke, K. (2019). Improving the LPJmL4-SPITFIRE vegetation-fire model for South America using satellite data. *Geoscientific Model Development*, *12*(12), 5029–5054. https://doi.org/10.5194/gmd-12-5029-2019

Duputié, A., Rutschmann, A., Ronce, O. & Chuine, I. (2015). Phenological plasticity will not help all species adapt to climate change. Global Change Biology, 21, 3062–3073

Forkel, M., Andela, N., P Harrison, S., Lasslop, G., Van Marle, M., Chuvieco, E., Dorigo, W., Forrest, M., Hantson, S., Heil, A., Li, F., Melton, J., Sitch, S., Yue, C. and Arneth, A. (2019): Emergent relationships with respect to burned area in global satellite observations and fire-enabled vegetation models, Biogeosciences, doi:10.5194/bg-16-57-2019

Forkel, M., Dorigo, W., Lasslop, G., Teubner, I., Chuvieco, E., & Thonicke, K. (2017). A data-driven approach to identify controls on global fire activity from satellite and climate observations (SOFIA V1). *Geoscientific Model Development*, *10*, 4443–4476. https://doi.org/10.5194/gmd-10-4443-2017

Forkel, M., Dorigo, W., Lasslop, G., Teubner, I., Chuvieco, E., & Thonicke, K. (2017). A data-driven approach to identify controls on global fire activity from satellite and climate observations (SOFIA V1). *Geoscientific Model Development*, *10*(12), 4443–4476. https://doi.org/10.5194/GMD-10-4443-2017

Garvey, S. M., Templer, P. H., Pierce, E. A., Reinmann, A. B. and Hutyra, L. R. (2021): Diverging patterns at the forest edge : Soil respiration dynamics of fragmented forests in urban and rural areas, 3094–3109, doi:10.1111/gcb.16099, 2022.

Gauzere, J., Teuf, B., Davi, H., Chevin, L.-M., Caignard, T., Leys, B., Delzon, S., Ronce, O. & Chuine, I. (2020). Where is the optimum? Predicting the variation of selection along climatic gradients and the adaptive value of plasticity. A case study on tree phenology. Evolution Letters, 4, 109–123.

GBIF. (2022). The global biodiversity information facility. URL https://www.gbif.org [accessed 24 January 2022]

Genikhovich, E.L., Sonkin, L.R., Kirillova, V.I., (2004). A statistical prognostic model for daily maxima of concentrations of urban air pollutnants, in: 9th Int.Conc. on Harmonisation within Atmospheric Dispersion Modelling for Regulatory Purposes. pp. 34–39

Guimberteau, M., Zhu, D., Maignan, F., Huang, Y., Yue, C., Dantec-N d lec, S., Ottl, C., Jornet-Puig, A., Bastos, A., Laurent, P., Goll, D., Bowring, S., Chang, J., Guenet, B., Tifafi, M., Peng, S., Krinner, G., Ducharne, A. s., Wang, F., Wang, T., Wang, X., Wang, Y., Yin, Z., Lauerwald, R., Joetzjer, E., Qiu, C., Kim, H. and Ciais, P. (2018): ORCHIDEE-MICT (v8.4.1), a land surface model for the high latitudes: model description and validation, Geosci. Model Dev., 11(1), 121–163, doi:10.5194/gmd-11-121-2018

Guo, D., Westra, S. & Maier, H.R. (2016). An R package for modelling actual, potential and reference evapotranspiration. Environmental Modelling & Software, 78, 216–224

Haas, O., Prentice, I. C. and Harrison, S. P. (2022): area , size , and intensity OPEN ACCESS Global environmental controls on wildfire burnt area , size , and intensity

 

Hansen, M.C., Potapov, P.V., Moore, R., Hancher, M., Turubanova, S.A., Tyukavina, A., Thau, D., Stehman, S.V., Goetz, S.J., Loveland, T.R., Kommareddy, A., Egorov, A., Chini, L., Justice, C.O., and Townshend, J.R.G., (2013): High-Resolution Global Maps of 21st-Century Forest Cover Change: Science, v. 342, no. 6160, p. 850-853

Hantson, S., Arneth, A., Harrison, S. P., Kelley, D. I., Colin Prentice, I., Rabin, S. S., Archibald, S., Mouillot, F., Arnold, S. R., Artaxo, P., Bachelet, D., Ciais, P., Forrest, M., Friedlingstein, P., Hickler, T., Kaplan, J. O., Kloster, S., Knorr, W., Lasslop, G., Li, F., Mangeon, S., Melton, J. R., Meyn, A., Sitch, S., Spessa, A., Van Der Werf, G. R., Voulgarakis, A. and Yue, C. (2016): The status and challenge of global fire modelling, Biogeosciences, doi:10.5194/bg-13-3359-2016

Hantson, S., Kelley, D. I., Arneth, A., Harrison, S. P., Archibald, S., Bachelet, D., Forrest, M., Hickler, T., Lasslop, G., Li, F., Mangeon, S., Melton, J. R., Nieradzik, L., Rabin, S. S., Colin Prentice, I., Sheehan, T., Sitch, S., Teckentrup, L., Voulgarakis, A. and Yue, C. (2020): Quantitative assessment of fire and vegetation properties in simulations with fire-enabled vegetation models from the Fire Model Intercomparison Project, Geosci. Model Dev., doi:10.5194/gmd-13-3299-2020

Hengl, T., Jesus, J.M. de, Heuvelink, G.B.M., Gonzalez, M.R., Kilibarda, M., Blagotic, A., Shangguan, Jalas, J. & Suominen, J. (1972–2005). Atlas florae europaeae. Committee for Mapping the Flora of Europe;Societas Biologica Fennica Vanamo, Helsinki, Finland

Keeth, J.J., Byram, G.M., (1968). A drought index for forest fire control (No. SE-38), USDA Forest service research paper. USDA - Forest Service Southearstern forest experimental station, Asheville

Krinner, G., Viovy, N., de Noblet-Ducoudré, N., Ogée, J., Polcher, J., Friedlingstein, P., Ciais, P., Sitch, S. and Prentice, I. C. (2005): A dynamic global vegetation model for studies of the coupled atmosphere-biosphere system, *Global Biogeochem. Cycles*, 19(1), doi:10.1029/2003GB002199

Kumar, V., Dharssi, I., (2015). Sources of soil dryness measures and forecasts for fire danger rating (No. 009), Bureau Research Report. *Australian government Bureau of Meteorology*

Laurent, P., Mouillot, F., Vanesa Moreno, M., Yue, C. and Ciais, P. (2019): Varying relationships between fire radiative power and fire size at a global scale, *Biogeosciences*, doi:10.5194/bg-16-275-2019

Lempereur M., Limousin J. M., Guibal F., Ourcival J. M., Rambal S., Ruffault J., Mouillot Florent. (2017). Recent climate hiatus revealed dual control by temperature and drought on the stem growth of Mediterranean Quercus ilex. *Global Change Biology*, 23 (1), p. 42-55. ISSN 1354-1013

Li, F., Val Martin, M., Andreae, M. O., Arneth, A., Hantson, S., Kaiser, J. W., Lasslop, G., Yue, C., Bachelet, D., Forrest, M., Kluzek, E., Liu, X., Mangeon, S., Melton, J. R., Ward, D. S., Darmenov, A., Hickler, T., Ichoku, C., Magi, B. I., Sitch, S., Van Der Werf, G. R., Wiedinmyer, C. and Rabin, S. S. (2019): Historical (1700-2012) global multi-model estimates of the fire emissions from the Fire Modeling Intercomparison Project (FireMIP), *Atmos. Chem. Phys*., doi:10.5194/acp-19-12545-2019

Lutz, F., Herzfeld, T., Heinke, J., Rolinski, S., Schaphoff, S., Von Bloh, W., Stoorvogel, J. J., & Müller, C. (2019). Simulating the effect of tillage practices with the global ecosystem model LPJmL (version 5.0-tillage). *Geoscientific Model Development*, *12*(6), 2419–2440. https://doi.org/10.5194/gmd-12-2419-2019

 

Maier, S.W., Russell-Smith, J., Edwards, A.C., Yates, C., (2013). Sensitivity of the MODIS fire detection algorithm (MOD14) in the savanna region of the Northern Territory, Australia. *ISPRS Journal of Photogrammetry and Remote Sensing* 76, 11–16. https://doi.org/10.1016/j.isprsjprs.2012.11.005

Mauri, A., Strona, G. & San-Miguel-Ayanz, J. (2017). EU-Forest, a high-resolution tree occurrence dataset for Europe. *Scientific Data*, 4, 160123.

Meeussen, C., Govaert, S., Vanneste, T., Bollmann, K., Brunet, J., Calders, K., Cousins, S. A. O., De Pauw, K., Diekmann, M., Gasperini, C., Hedwall, P. O., Hylander, K., Iacopetti, G., Lenoir, J., Lindmo, S., Orczewska, A., Ponette, Q., Plue, J., Sanczuk, P., Selvi, F., Spicher, F., Verbeeck, H., Zellweger, F., Verheyen, K., Vangansbeke, P. and De Frenne, P. (2021): Microclimatic edge-to-interior gradients of European deciduous forests*, Agric. For. Meteorol.,* 311(May), doi:10.1016/j.agrformet.2021.108699

Meeussen, C., Govaert, S., Vanneste, T., Calders, K., Bollmann, K., Brunet, J., Cousins, S. A. O., Diekmann, M., Graae, B. J., Hedwall, P. O., Krishna Moorthy, S. M., Iacopetti, G., Lenoir, J., Lindmo, S., Orczewska, A., Ponette, Q., Plue, J., Selvi, F., Spicher, F., Tolosano, M., Verbeeck, H., Verheyen, K., Vangansbeke, P. and De Frenne, P. (2020): Structural variation of forest edges across Europe, *For. Ecol. Manage.,* 462(January), 117929, doi:10.1016/j.foreco.2020.117929

Meijer, J. R., Huijbregts, M. A. J., Schotten, K. C. G. J. and Schipper, A. M. (2018): Global patterns of current and future road infrastructure, *Environ. Res. Lett*., 13(6), doi:10.1088/1748-9326/aabd42

Meinshausen, M., Nicholls, Z. R. J., Lewis, J., Gidden, M. J., Vogel, E., Freund, M., Beyerle, U., Gessner, C., Nauels, A., Bauer, N., Canadell, J. G., Daniel, J. S., John, A., Krummel, P. B., Luderer, G., Meinshausen, N., Montzka, S. A., Rayner, P. J., Reimann, S., Smith, S. J., van den Berg, M., Velders, G. J. M., Vollmer, M. K., and Wang, R. H. J., (2020): The shared socio-economic pathway (SSP) greenhouse gas concentrations and their extensions to 2500. *Geosci. Model Dev*. 13, 3571–3605. https://doi.org/10.5194/gmd-13-3571-2020, 2020

Monnet, A.-C., Cilleros, K., Médail, F., Albassatneh, M.C., Arroyo, J., Bacchetta, G., Bagnoli, F., Barina, Z., Cartereau, M., Casajus, N., Dimopoulos, P., Domina, G., Doxa, A., Escudero, M., Fady, B., Hampe, A., Matevski, V., Misfud, S., Nikolic, T., Pavon, D., Roig, A., Barea, E.S., Spanu, I., Strid, A.,

Moreira, F., Viedma, O., Arianoutsou, M., Curt, T., Koutsias, N., Rigolot, E., Barbati, A., Corona, P., Vaz, P., Xanthopoulos, G., Mouillot, F., & Bilgili, E. (2011). Landscape – wildfire interactions in southern Europe: Implications for landscape management. *Journal of Environmental Management*, *92*(10), 2389–2402. https://doi.org/10.1016/J.JENVMAN.2011.06.028

Morin, X., Augspurger, C. & Chuine, I. (2007). Process-Based Modeling of Species' Distributions: What Limits Temperate Tree Species' Range Boundaries? Ecology, 88, 2280–2291.

Morreale, L. L., Thompson, J. R., Tang, X., Reinmann, A. B. and Hutyra, L. R. (2021): Elevated growth and biomass along temperate forest edges, *Nat. Commun.,* 12(1), doi:10.1038/s41467-021-27373-7

Mouillot F., Rambal S., LAvorel S. (2001). A generic process-based SImulator for meditERRanean landscApes (SIERRA): design and validation exercises*. Forest Ecology and Management*. Volume 147, Issue 1, 15 June 2001, Pages 75-97

Muñoz Sabater, J., (2019): ERA5-Land hourly data from 1981 to present. Copernicus Climate Change Service (C3S) Climate Data Store (CDS). (Accessed on < DD-MMM-YYYY >), 10.24381/cds.e2161bac

 

Muñoz Sabater, J., (2021): ERA5-Land hourly data from 1950 to 1980. Copernicus Climate Change Service (C3S) Climate Data Store (CDS). (Accessed on < DD-MMM-YYYY >), 10.24381/cds.e2161bac

P. Potapov, X. Li, A. Hernandez-Serna, A. Tyukavina, M.C. Hansen, A. Kommareddy, A. Pickens, S. Turubanova, H. Tang, C.E. Silva, J. Armston, R. Dubayah, J. B. Blair, M. Hofton (2020): Mapping and monitoring global forest canopy height through integration of GEDI and Landsat data. *Remote Sensing of Environment,* 112165

Randerson, J. T., D, line 319 to 325 Van, er Werf, G. R., Giglio, L., Collatz, G. J., & Kasibhatla, P. S. (2017). *Global Fire Emissions Database, Version 4.1 (GFEDv4)*. ORNL Distributed Active Archive Center. https://doi.org/10.3334/ORNLDAAC/1293

Ritenberga, O., Sofiev, M., Kirillova, V., Kalnina, L., Genikhovich, E., (2016). Statistical modelling of non-stationary processes of atmospheric pollution from natural sources: Example of birch pollen. *Agricultural and Forest Meteorology* 226–227, 96–107. https://doi.org/10.1016/j.agrformet.2016.05.016

Ritenberga, O., Sofiev, M., Siljamo, P., Saarto, A., Dahl, A., Ekebom, A., Sauliene, I., Shalaboda, V., Severova, E., Hoebeke, L., Ramfjord, H., (2018). A statistical model for predicting the inter-annual variability of birch pollen abundance in Northern and North-Eastern Europe. Science of The Total Environment 615, 228-239. https://doi.org/10.1016/j.scitotenv.2017.09.061

Rogers, B. M., Soja, A. J., Goulden, M. L. and Randerson, J. T. (2015): Influence of tree species on continental differences in boreal fires and climate feedbacks, *Nat. Geosci.,* doi:10.1038/ngeo2352

Rothermel, R. C. (1972). A mathematical model for predicting fire spread in wildland fuels. *Res. Pap. INT-115. Ogden, UT: U.S. Department of Agriculture, Intermountain Forest and Range Experiment Station. 40 P.*, *115*, 40. https://www.fs.usda.gov/research/treesearch/32533

Rothermel, R. C.(1991): Predicting behavior and size of crown fires in the northern Rocky Mountains, USDA For. *Serv. Intermt. Res. Station. Res. Pap.*, (January), 46

Saltré, F., Saint-Amant, R., Gritti, E.S., Brewer, S., Gaucherel, C., Davis, B.A.S. & Chuine, I. (2013). Climate or migration: What limited European beech post-glacial colonization? *Global Ecology and Biogeography*, 22, 1217–1227.

Schaphoff, S., Von Bloh, W., Rammig, A., Thonicke, K., Biemans, H., Forkel, M., Gerten, D., Heinke, J., Jägermeyr, J., Knauer, J., Langerwisch, F., Lucht, W., Müller, C., Rolinski, S., & Waha, K. (2018). LPJmL4 - A dynamic global vegetation model with managed land - Part 1: Model description. *Geoscientific Model Development*, *11*(4), 1343–1375. https://doi.org/10.5194/gmd-11-1343-2018

Schreck, M.-B., Howerton, P.J., Cook, K.R., 2010. Adapting Australia's Grassland Fire Danger Index for the United States' Central Plains 19

Scoccimarro, E., & Navarra, A. (2022). Precipitation and Temperature Extremes in a Changing Climate. In *Hydrometeorological Extreme Events and Public Health* (pp. 3–25). John Wiley & Sons, Ltd. https://doi.org/10.1002/9781119259350.ch2

Simpson, K. J., Jardine, E. C., Archibald, S., Forrestel, E. J., Lehmann, C. E. R., Thomas, G. H. and Osborne, C. P. (2021): Resprouting grasses are associated with less frequent fire than seeders, New Phytol., 230(2), 832–844, doi:10.1111/nph.17069

 

Soares, J., Sofiev, M., Hakkarainen, J., (2015). Uncertainties of wild-land fi res emission in AQMEII phase 2 case study. *Atmospheric Environment* 115, 361-370. https://doi.org/10.1016/j.atmosenv.2015.01.068

Sofiev, M., Ermakova, T., Vankevich, R., (2012). Evaluation of the smoke-injection height from wild-land fires using remote-sensing data. *Atmospheric Chemistry and Physics* 12, 1995–2006. https://doi.org/10.5194/acp-12-1995-2012

Sofiev, M., Ritenberga, O., Albertini, R., Arteta, J., Belmonte, J., Bonini, M., Celenk, S., Damialis, A., Douros, J., Elbern, H., Friese, E., Galan, C., Gilles, O., Hrga, I., Kouznetsov, R., Krajsek, K., Plu, M., Prank, M., Robertson, L., Steensen, B.M., Thibaudon, M., Segers, A., Stepanovich, B., Valdebenito, A.M., Vira, J., Vokou, D., (2017). Multi - model ensemble simulations of olive pollen distribution in Europe in 2014 . *Atmospheric Chemistry and Physics Discussions*. https://doi.org/10.5194/acp-2016-1189

Sofiev, M., Vankevich, R., Lotjonen, M., Prank, M., Petukhov, V., Ermakova, T., Koskinen, J., Kukkonen, J., (2009): An operational system for the assimilation of the satellite information on wild-land fires for the needs of air quality modelling and forecasting. *Atmospheric Chemistry and Physics* 9, 6833–6847

Stenzel, J. E., Bartowitz, K. J., Hartman, M. D., Lutz, J. A., Kolden, C. A., Smith, A. M. S., Law, B. E., Swanson, M. E., Larson, A. J., Parton, W. J. and Hudiburg, T. W. (2019): Fixing a snag in carbon emissions estimates from wildfires, *Glob. Chang. Biol.,* doi:10.1111/gcb.14716

Thonicke, K., Spessa, A., Prentice, I. C., Harrison, S. P., Dong, L., & Carmona-Moreno, C. (2010). The influence of vegetation, fire spread and fire behaviour on biomass burning and trace gas emissions: results from a process-based model. *Biogeosciences*, *7*, 1991-2011. https://doi.org/10.5194/bg-7-1991-2010

Thonicke, K., Spessa, A., Prentice, I. C., Harrison, S. P., Dong, L. and Carmona-Moreno, C. (2010): The influence of vegetation, fire spread and fire behaviour on biomass burning and trace gas emissions: Results from a process-based model, *Biogeosciences,* doi:10.5194/bg-7-1991-2010

Thonicke, K., Spessa, A., Prentice, I. C., Harrison, S. P., Dong, L., & Carmona-Moreno, C. (2010). The influence of vegetation, fire spread and fire behaviour on biomass burning and trace gas emissions: Results from a process-based model. *Biogeosciences*, *7*(6), 1991–2011. https://doi.org/10.5194/bg-7-1991-2010

Tóth, B., Weynants, M., Pásztor, L. & Hengl, T. (2017). 3D soil hydraulic database of Europe at 250 m, *Wiley Online Library,* doi: 10.1002/hyp.11203.

Trautmann, H., Mersmann, O. & Arnu, D. (2011). Cmaes: Covariance matrix adapting evolutionary strategy

Van Marle, M. J. E., Kloster, S., Magi, B. I., Marlon, J. R., Daniau, A. L., Field, R. D., Arneth, A., Forrest, M., Hantson, S., Kehrwald, N. M., Knorr, W., Lasslop, G., Li, F., Mangeon, S., Yue, C., Kaiser, J. W. and Van Der Werf, G. R. (2017): Historic global biomass burning emissions for CMIP6 (BB4CMIP) based on merging satellite observations with proxies and fire models (1750-2015), *Geosci. Model Dev.,* doi:10.5194/gmd-10-3329-2017

van Nes EH, Staal A, Hantson S, Holmgren M, Pueyo S, Bernardi RE, et al. (2018): Fire forbids fifty-fifty forest. *PLoS ONE* 13(1): e0191027. https://doi.org/10.1371/journal.pone.0191027

Van Wagner, C.E., Pickett, T.L., (1985). Equations and FORTRAN program for the Canadian Forest Fire Weather Index System (No. 33), Forestry technical report*. Canadian Forestry Service,* Ottawa, Canada

Vendramin, G.G. & Leriche, A. (2021). WOODIV, a database of occurrences, functional traits, and phylogenetic data for all Euro-Mediterranean trees. *Scientific Data*, 8, 89.

 

Von Bloh, W., Schaphoff, S., Müller, C., Rolinski, S., Waha, K., & Zaehle, S. (2018). Implementing the nitrogen cycle into the dynamic global vegetation, hydrology, and crop growth model LPJmL (version 5.0). *Geoscientific Model Development*, *11*(7), 2789–2812. https://doi.org/10.5194/GMD-11-2789-2018

W., Wright, M.N., Geng, X., Bauer-Marschallinger, B., Guevara, M.A., Vargas, R., MacMillan, R.A.,

Ward, D. S., Shevliakova, E., Malyshev, S. and Rabin, S. (2018): Trends and Variability of Global Fire Emissions Due To Historical Anthropogenic Activities, *Global Biogeochem. Cycles*, 32(1), 122–142, doi:10.1002/2017GB005787

Wooster, M., (2003). Fire radiative energy for quantitative study of biomass burning: derivation from the BIRD experimental satellite and comparison to MODIS fire products. *Remote Sensing of Environment* 86, 83–107. https://doi.org/10.1016/S0034-4257(03)00070-1

Yue, C., Ciais, P., Cadule, P., Thonicke, K. and Van Leeuwen, T. T. (2015a): Modelling the role of fires in the terrestrial carbon balance by incorporating SPITFIRE into the global vegetation model ORCHIDEE -Part 2: Carbon emissions and the role of fires in the global carbon balance, Geosci. Model Dev., doi:10.5194/gmd-8-1321-2015

Yue, C., Ciais, P., Cadule, P., Thonicke, K. and Van Leeuwen, T. T. (2015b): Modelling the role of fires in the terrestrial carbon balance by incorporating SPITFIRE into the global vegetation model ORCHIDEE -Part 2: Carbon emissions and the role of fires in the global carbon balance, *Geosci. Model Dev*., 8(5), 1321–1338, doi:10.5194/gmd-8-1321-2015,

Yue, C., Ciais, P., Cadule, P., Thonicke, K., Archibald, S., Poulter, B., Hao, W. M., Hantson, S., Mouillot, F., Friedlingstein, P., Maignan, F. and Viovy, N. (2014): Modelling the role of fires in the terrestrial carbon balance by incorporating SPITFIRE into the global vegetation model ORCHIDEE - Part 1: Simulating historical global burned area and fire regimes, *Geosci. Model Dev*., doi:10.5194/gmd-7-2747-2014

Zheng, B., Ciais, P., Chevallier, F., Chuvieco, E., Chen, Y. and Yang, H. (2014): Increasing forest fire emissions despite the decline in global burned area, *Sci. Adv., 7*(39), doi:10.1126/sciadv.abh2646

Zhu, D., Peng, S. S., Ciais, P., Viovy, N., Druel, A., Kageyama, M., Krinner, G., Peylin, P., Ottlé, C., Piao, S. L., Poulter, B., Schepaschenko, D. and Shvidenko, A. (2015): Improving the dynamics of Northern Hemisphere high-latitude vegetation in the ORCHIDEE ecosystem model, *Geosci. Model Dev.*, doi:10.5194/gmd-8-2263-2015

Zhu, D., Peng, S., Ciais, P., Zech, R., Krinner, G., Zimov, S. and Grosse, G. (2016): Simulating soil organic carbon in yedoma deposits during the Last Glacial Maximum in a land surface model, *Geophys. Res. Lett*., 43(10), 5133–5142, doi:10.1002/2016GL068874

 

# List of tables



# List of Figures



 

 

 